Polymer Testing 140 (2024) 108594

Contents lists available at ScienceDirect

Polymer Testing

journal homepage: www.elsevier.com/locate/polytest

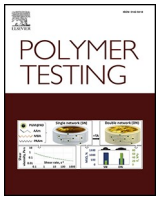

A new strategy applying ternary blends of modified natural rubber with fluoroplastic and fluorocarbon elastomer for high-performance thermoplastic vulcanizate

Subhan Salaeh [a,b,*], Anoma Thitithammawong [a,b], Shib Shankar Banerjee [c]

[a] Department of Rubber Technology and Polymer Science, Faculty of Science and Technology, Prince of Songkla University, Pattani Campus, Pattani, 94000, Thailand
[b] Research Unit of Advanced Elastomeric Materials and Innovations for BCG Economy (AEMI), Faculty of Science and Technology, Prince of Songkla University, Pattani Campus, Thailand
[c] Department of Materials Science and Engineering, Indian Institute of Technology Delhi, New Delhi, 110016, India

ARTICLE INFO

Keywords:
Poly(vinylidene fluoride)
Fluorocarbon elastomer
Natural rubber
High-performance
Ternary blend
Thermoplastic vulcanizate
Compatibilization

ABSTRACT

High-performance thermoplastic vulcanizates (TPVs) are a class of specialty polymers with exceptional mechanical properties, rubber-like elasticity, excellent processability and recyclability, and an excellent price-performance ratio that make them ideal for a variety of industrial applications. In this work, a successful method of creating high-performance TPV using a ternary blend of poly(methyl methacrylate) modified natural rubber (MGNR), poly(vinylidene fluoride) (PVDF), and fluorocarbon elastomer (FKM) was employed. Combining NR known for its exceptional rubber elasticity and resilience, with fluoropolymers, known for their exceptional chemical resistance and thermal stability, resulted in materials with a synergistic blend of properties. The developed PVDF/FKM/MGNR blend showed higher elasticity, tensile strength, and elongation at break than PVDF/FKM and PVDF/MGNR blends because the ternary blend had greatly improved phase morphology and compatibility between the three phases. The domain size in the ternary blend was smaller than 150 nm. The ternary blends also exhibited excellent thermal properties, where melting and crystallization temperatures were reduced significantly with MGNR due to possible dipole-dipole interactions. At the same time, the oil resistance and shape memory behavior of PVDF/FKM/MGNR were improved at an appropriate blend ratio. The ternary TPVs demonstrated good shape fixities (90–100 %) and shape recoveries (70–80 %). This research offers valuable insights into the design of high-performance thermoplastic elastomers based on natural rubber, which have excellent mechanical properties, solvent resistance, and potential for intelligent and lightweight application.

1. Introduction

Natural rubber (NR) is a renewable bio-elastomer consisting of 99 % of cis-1,4-polyisoprene. This renewable rubber is extracted as latex from the rubber tree *Hevea Brasiliensis*. The high cis configuration of NR makes it extraordinarily elastic and has excellent mechanical properties. So, the unfilled NR vulcanizate exhibits high tensile strength, tear strength, and elongation at break without reinforcing fillers. However, unmodified NR has critical limitations in functional and advanced applications due to the hydrocarbon structure and unsaturated C=C groups. These cause it to have poor oil resistance and low thermal stability, with poor resistance also to degradation induced by oxygen and ozone [1,2]. Therefore, many chemical modification techniques have been investigated to improve the polarity, oil resistance, thermal stability, and degradation resistance of NR, such as epoxidation [3–5], graft copolymerization [6–8], and hydrogenation [9]. These techniques reduced unsaturation in the structure and introduced new functional groups to the NR backbone. However, a single strategy may not achieve the properties desired in a particular application. Blending chemically modified natural rubber with thermoplastic can boost the mechanical, chemical, and thermal properties of natural rubber [10–12].

Thermoplastic elastomers (TPEs) have received a significantly growing interest in the field of elastomeric-like materials and offer excellent processability and recyclability. TPEs mainly consist of hard and soft domains to offer exceptional mechanical strength and elasticity. Thus, various methods for designing the hard and soft segments for TPEs

* Corresponding author. Department of Rubber Technology and Polymer Science, Faculty of Science and Technology, Prince of Songkla University, Pattani Campus, Pattani, 94000, Thailand.
E-mail address: subhan.s@psu.ac.th (S. Salaeh).

https://doi.org/10.1016/j.polymertesting.2024.108594
Received 30 April 2024; Received in revised form 29 August 2024; Accepted 23 September 2024
Available online 24 September 2024

Table 1
Compositions of thermoplastic elastomers derived from PVDF/FKM/MGNR.

Ingredient	Quantity (parts per hundred of polymer, php)	
	PVDF/FKM/MGNR TPE	PVDF/FKM/MGNR TPV
PVDF/FKM/MGNR[a]	100	100
Antioxidant	1.5	1.5
MgO	–	3.0
HMDC	–	5.0

[a] The blends were prepared with different proportions.

have been reported in the literature. In fact, two main groups of TPEs have been studied to combine thermoplastic character with rubber elasticity: i) block copolymers such as styrene block copolymer, polyamide block copolymer, polyurethane multiblock copolymer, and polyester block copolymer, ii) the blending of thermoplastic and rubber to make thermoplastic elastomer (TPE) or thermoplastic vulcanizate (TPV). In TPVs, the rubber phase is vulcanized, and the resulting materials generally show excellent elasticity, mechanical strength, chemical resistance, processability, and recyclability [13,14]. The first commercial TPV based on PP/EPDM was first launched in 1981 by Monsanto under the trade name Santoprene®. Further on, many explorations have shown the possibility of preparing TPV from various types of rubbers and plastics to achieve optimum properties for specific practical applications. Natural rubber (NR) and modified NR are extensively used to prepare TPV by blending with various types of thermoplastic, such as polypropylene (PP) [10,15,16], polyethylene (PE) [17,18], polystyrene (PS) [19], polylactic acid (PLA) [20,21], etc.

Recent developments in TPVs focus on high performance, 3D printing, shape memory and smart applications [22–24]. Oil and solvent resistance remain the main challenges in making high-performance TPVs. Particularly, thermoplastics like polyamide and rubber, that is, acrylonitrile butadiene rubber (NBR) and hydrogenated acrylonitrile butadiene rubber (HNBR), have been selected to develop oil and heat-resistant TPVs [13,25–27]. To further increase oil resistance and smart characteristics of TPV, fluorine-containing polymers, such as polyvinylidene fluoride (PVDF) and fluorocarbon elastomer (FKM), have also been used to develop advanced functional TPEs and TPVs. Interestingly, PVDF is a kind of polymer containing vinylidene fluoride homopolymers having excellent weather resistance, chemical resistance, and strong mechanical properties. At the same time, PVDF is well-known for its smart electro-active polymer and piezoelectric properties. FKM, a fluorocarbon copolymer based on vinylidene fluoride (VDF), hexafluoropropylene (HFP), tetrafluoroethylene (TFE), and chlorotrifluoroethylene (CTFE), is a specialty synthetic elastomer with outstanding weather, oil, hydrocarbon solvent, and heat resistances [28]. Owing to the fluorine atoms in the main chains of PVDF and FKM, they are good candidates for the preparation of oil and heat-resistant TPVs [29–31]. For example, Guo et al. prepared fluorocarbon elastomer (FKM)/fluoro-thermoplastic (EFEP) TPV with rubber phase domain diameter in the range of 370–880 nm, depending on the viscosity ratio of blend components. The FKM/EFEP TPV also showed good mechanical properties, elasticity, recyclability, oil resistance, and gas barrier properties [29].

The developments of high-performance, shape memory, heat-resistant, and oil-resistant TPVs based on NR are rarely studied because NR exhibits poor oil resistance and shape fixity. Meanwhile, NR's high degree of unsaturation offers less resistance to thermal oxidation and decomposition. Improving those properties by blending with fluorinated polymers and elastomers (i.e., PVDF and FKM) is severely challenged due to the non-polar hydrocarbon structure of NR, resulting in poor compatibility and inferior physical and chemical properties. However, compatibility of PVDF with NR can be improved by using modified NRs such as, epoxidized natural rubber (ENR) [32,33] and poly(methyl methacrylate) modified natural rubber (MGNR) [12]. Recently, ENR has been proven to have structural compatibility for fluorinated thermoplastic because it offered improved compatibility with PVDF as compared to unmodified NR, and interfacial adhesion was significantly enhanced by the epoxide groups in ENR [33,34]. In our previous works, high dielectric constant TPVs were successfully fabricated based on PVDF/ENR50 blends filled with barium titanate. The TPV/barium titanate composite with higher PVDF proportion showed higher permittivity because PVDF has a strong dipole moment of the CF_2 segments [35]. Moreover, we also found that NR-grafted-PMMA (MGNR) showed good compatibility with PVDF due to dipole-dipole interactions between grafted PMMA and fluorine groups in PVDF [12]. Therefore, PVDF/MGNR TPV showed improved mechanical and morphological properties.

In this work, an effective strategy was implemented to fabricate a high-performance thermoplastic vulcanizate from ternary blends of poly (methyl methacrylate) modified natural rubber (MGNR), poly(vinylidene fluoride) (PVDF), and fluorocarbon elastomer (FKM). These three components in the TPV can provide different specific properties. For example, PVDF provides strength, recyclability, heat resistance, and oil resistance. Blending FKM in the blend allows for improving dynamic vulcanization and resistance to heat and solvents. At the same time, MGNR is known for good dipole-dipole interactions with PVDF, as described in our previous report [12]. The MGNR can improve morphology and shape fixity. The blending of these three components can be a new strategy for producing a multifunctional TPV with excellent oil resistance, heat resistance, and shape memory behavior. Poly (methyl methacrylate) modified natural rubber (MGNR) was first synthesized via emulsion polymerization to improve compatibility with FKM and PVDF. Melt mixing of MGNR with PVDF and FKM was performed without curative to prepare TPE. TPV was prepared through dynamic vulcanization using a diamine for curing to establish a chemical cross-link between FKM and MGNR. Phase morphology and compatibility between phase components of TPE and TPV were accessed. Subsequently, dynamic mechanical analysis, crystallinity, heat resistance, and shape memory performance were systematically studied. This work provides a promising method to advance the understanding of high-performance TPV design and its multifaceted applicability in industrial sectors.

2. Experimental procedure

2.1. Materials

Polyvinylidene fluoride (PVDF) (KYNAR® 740) was manufactured by Arkema, France. Fluorocarbon elastomer (FKM) by the trade name of MLF 2–11 [fluorine content: 66 % and ML(1 + 10) at 121 °C: 25 Mooney unit] was manufactured by Jiangsu Meilan Chemical Co., Ltd. (China). Hexamethylenediamine carbamate (Rhonocure® HMDC) was manufactured by LANXESS AG (Germany). Magnesium oxide (MgO) was purchased from Acros Organics. Antioxidant 1010 (JYANOX-1010) was manufactured by Jiyi Chemical Co., Ltd (China).

2.2. Preparation of MGNR

MGNR used in this work was prepared by graft copolymerization between NR latex and 40 wt% of methyl methacrylate (MMA) monomer. This was done by emulsion polymerization technique following our previous work [12]. The free NR, free PMMA, and grafting efficiency (GE) investigated by Soxhlet extraction were about 5.0 %, 11.7 %, and 83.8 %, respectively.

2.3. Preparation of ternary blend and thermoplastic vulcanizate

The PVDF/FKM/MGNR40 blends with different proportions by weight were melt-mixed using Brabender plasticorder at 180 °C and 60 rpm. The thermoplastic elastomers (TPEs) were prepared without a curing agent, whereas thermoplastic vulcanizates (TPVs) were prepared

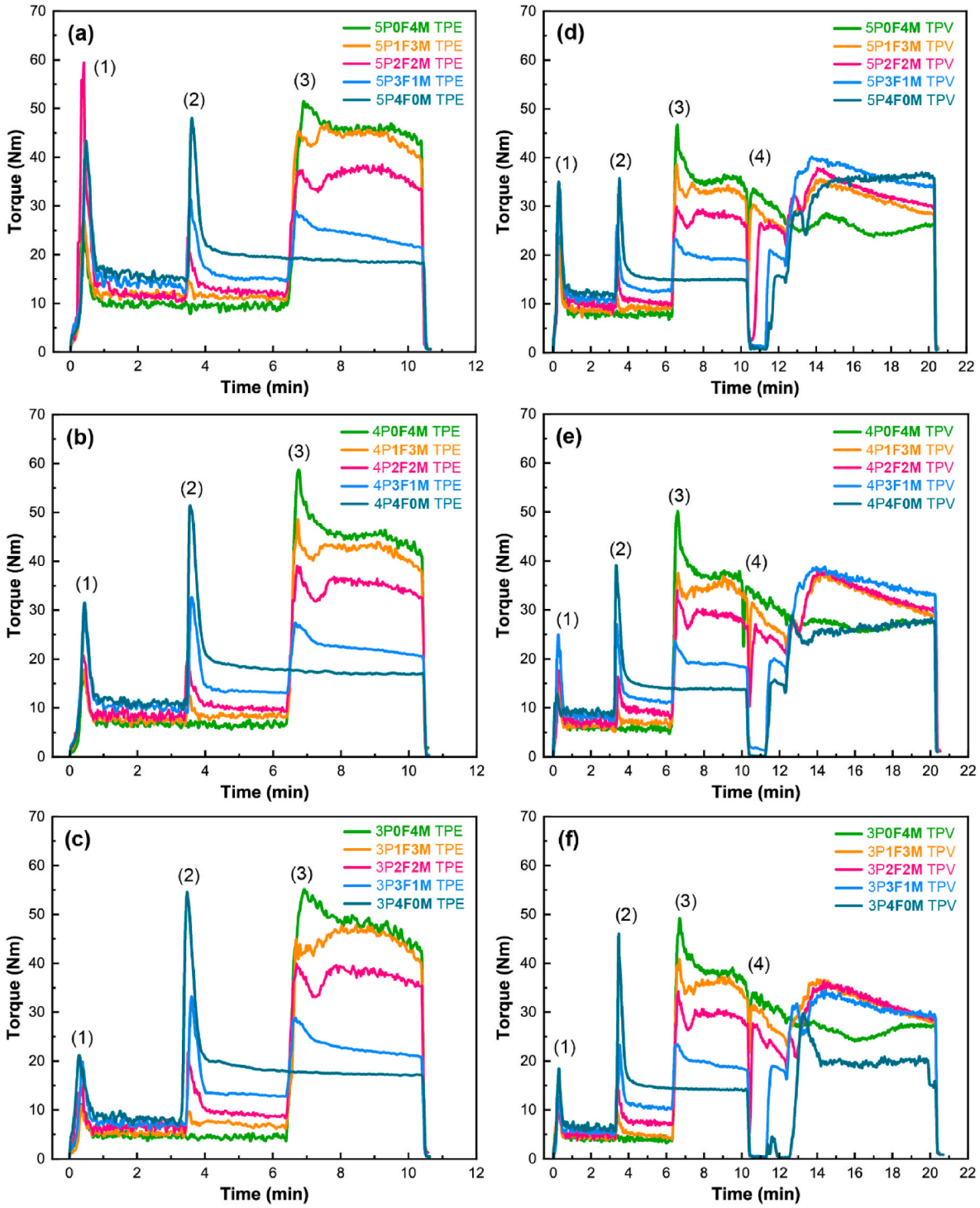

Fig. 1. The mixing torques for (a, b, c) PVDF/FKM/MGNR TPE and (d, e, f) PVDF/FKM/MGNR TPV with different blend ratios at 200 °C and 60 rpm. The numbers (1), (2), (3), and (4) indicate the additions of PVDF, FKM, MGNR, and curative respectively.

using dynamic vulcanization with a curing agent, as shown in Table 1. After blending, TPE and TPV sheets (120 x 120 × 1.5 mm^3) were prepared by compression molding. The samples were preheated and pressed at a temperature of 200 °C for 40 min, and the sheets were then cooled down for 20 min to room temperature by circulating water.

In this work, the PVDF to rubbers ratio was varied among 50/50, 40/60, and 30/70 wt%. In the rubber proportion, the FKM:MGNR ratio was varied among 0:4, 1:3, 2:2, 3:1, and 4:0. The code labels for all these blends are described next.

1. At a blend ratio of 50 wt% of PVDF (**5P**) and 50 wt% rubber, the mass ratio PVDF/FKM/MGNR was varied among 50/0/50, 50/12.5/37.5, 50/25/25, 50/37.5/12.5, and 50/50/0 wt%, which are denoted by **5P0F4M**, **5P1F3M**, **5P2F2M**, **5P3F1M**, and **5P4F0M**, respectively.
2. At a blend ratio of 40 wt% of PVDF (**4P**) to 60 wt% rubber, the mass ratio PVDF/FKM/MGNR was varied among 40/0/60, 40/15/45, 40/30/30, 40/45/15, and 40/60/0 wt%, which are denoted by **4P0F4M**, **4P1F3M**, **4P2F2M**, **4P3F1M**, and **4P4F0M**, respectively.
3. At a blend ratio of 30 wt% of PVDF (**3P**) to 70 wt% rubber, the mass ratio PVDF/FKM/MGNR was varied among 30/0/70, 30/17.5/52.5,

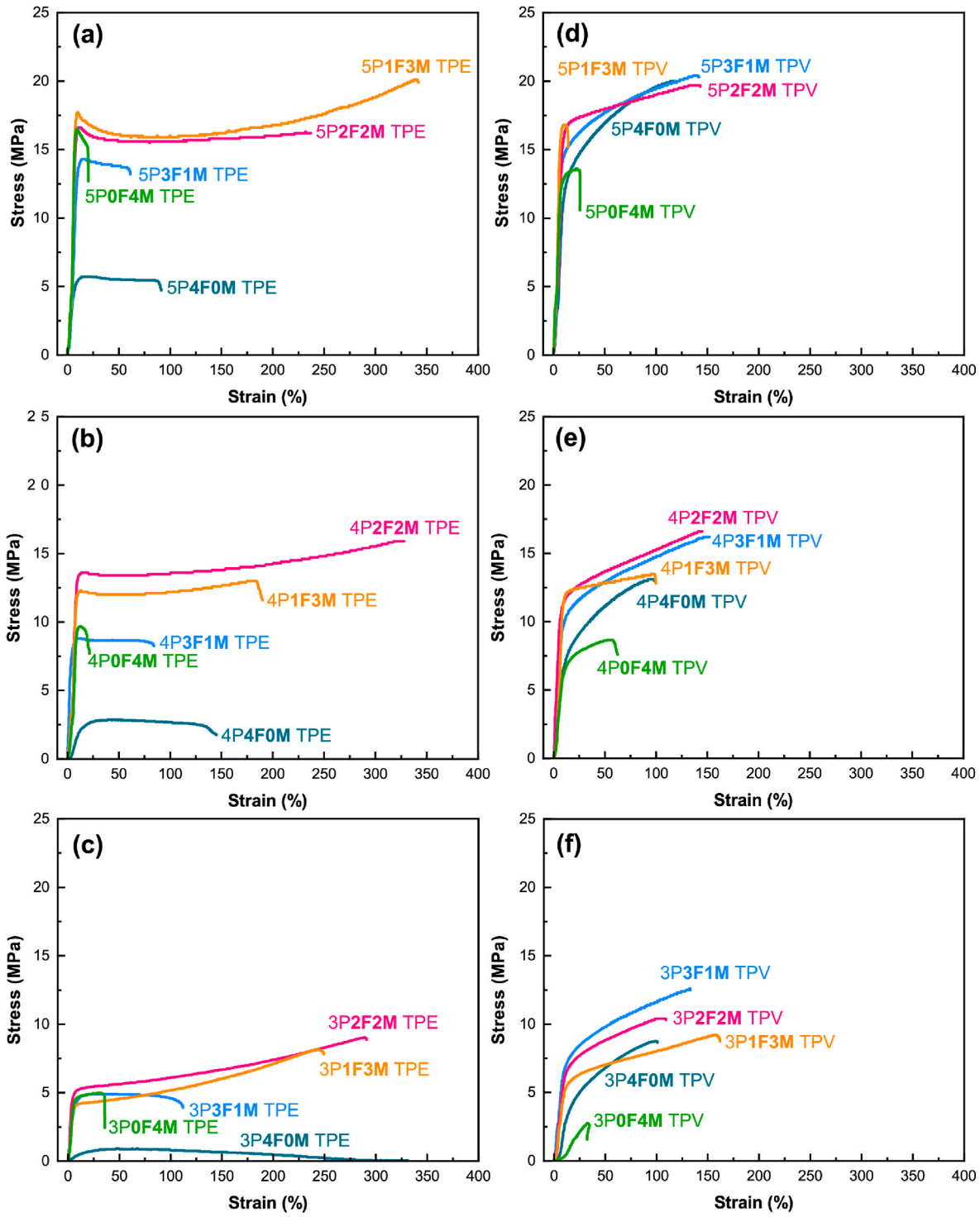

Fig. 2. Stress-stain curves of (a–c) PVDF/FKM/MGNR TPE, and (d–f) TPV with different blend ratios of PVDF/Rubber: (a and d) 50 wt% PVDF (**5P**), (b and e) 40 wt% PVDF (**4P**), and (c and f) 30 wt% PVDF (**3P**).

30/35/35, 30/52.5/17.5, and 30/70/0 wt%, which are denoted by **3P0F4M**, **3P1F3M**, **3P2F2M**, **3P3F1M**, and **3P4F0M**, respectively.

2.4. Characterizations

Mechanical properties. The stress-strain behavior was studied for all the blends using a universal tensile testing machine (Hounsfield Tensometer, model H 10 KS, Hounsfield Test Equipment Co., Surrey, UK) according to ISO37. All cases were measured with a 5 kN load cell and a strain rate of 200 mm/min.

Morphological analysis. The phase morphology of unetched PVDF/FKM/MGNR blends was assessed using a scanning electron microscope (SEM) (Quanta 400, Thermo Fisher Scientific, Czech Republic) at an acceleration voltage of 20 kV. The cryo-fractured surface was stained with osmium tetroxide (OsO_4) and coated with a thin layer of gold. The morphology of PVDF/FKM/MGNR ternary blends was also evaluated using a transmission electron microscope (TEM) (Talos F200i, Thermo Fisher Scientific, Czech Republic) at an acceleration voltage of 200 kV.

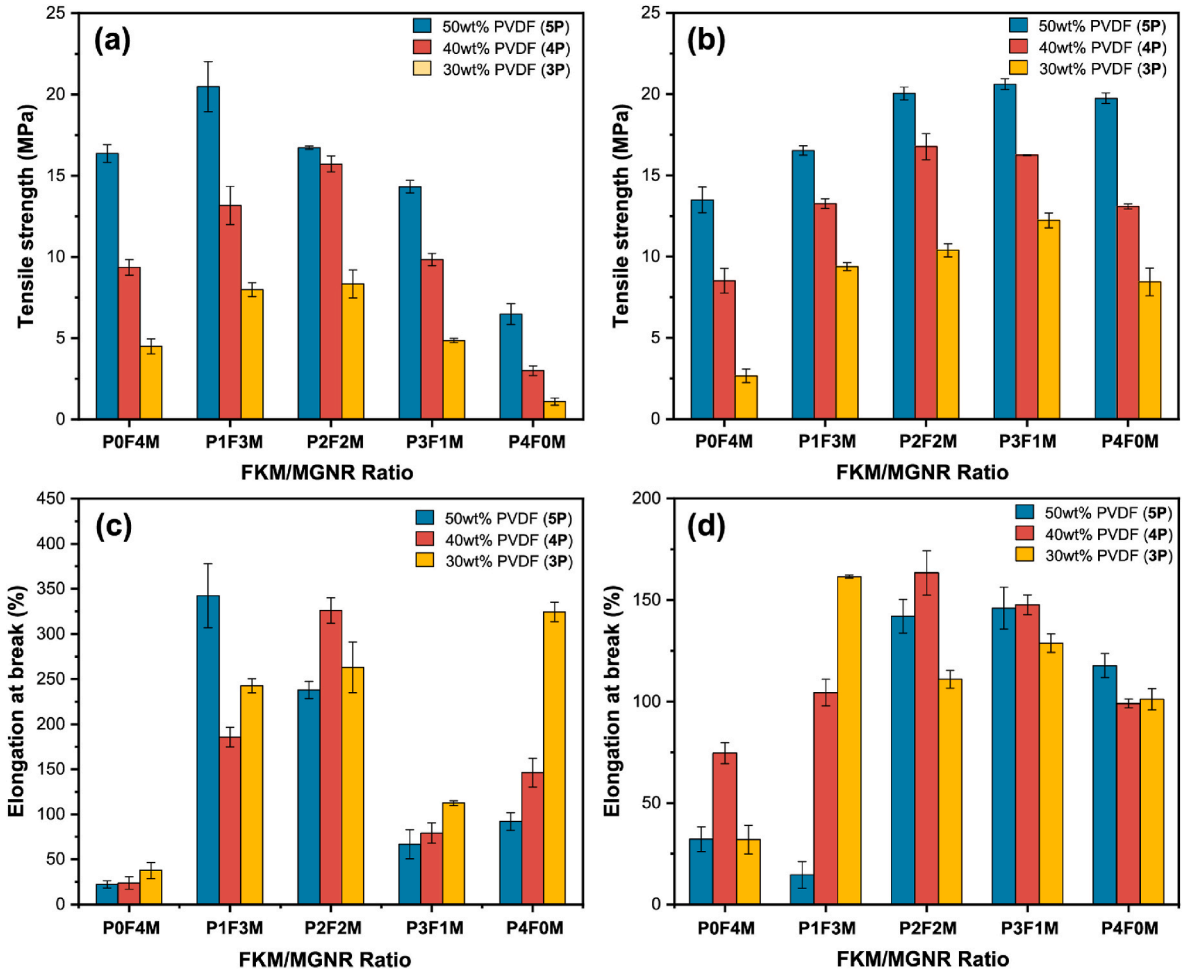

Fig. 3. Mechanical properties of PVDF/FKM/MGNR40 blends: (a, c) thermoplastic elastomers (TPEs), and (b, d) thermoplastic vulcanizates (TPVs).

The cryosectioned samples with a thickness of about 60 nm used for TEM observation were prepared using an ultramicrotome (MT-XL, RMC Boeckeler, USA). The TEM observation was performed without straining. The domain diameter was determined from three independent SEM images using ImageJ software, where number-average domain size (D_n) and weight-average domain size (D_w) were calculated using the following **Equations 1** and **2**, respectively [36,37].

$$D_n = \frac{\sum_i n_i D_i}{\sum_i n_i} \quad (1)$$

$$D_w = \frac{\sum_i n_i D_i^2}{\sum_i n_i D_i} \quad (2)$$

Where n_i is the number of particles that have the particle diameter D_i.

Morphology of TPVs was also observed using an atomic force microscope (AFM). Before AFM measurement, the smooth surface of the blends was cryogenically cut by ultramicrotome (MT-XL, RMC Boeckeler, USA) with a glass knife at −100 °C. The AFM images were captured at room temperature in the tapping mode with phase imaging using FlexAFM (Nanosurf, Switzerland).

Dynamic mechanical analysis. The storage modulus (E') and tan δ of TPE and TPV were analyzed by a dynamic mechanical analyzer (DMA) (DMA850, TA Instrument, USA). The measurement was performed in tension mode within the temperature range from −80 to 180 °C at a heating rate of 2 K/min and a frequency of 10 Hz.

Rheological behavior. The measurements of rheological properties of the mixtures were performed with a Rubber Process Analyzer (RPA 2000, Alpha Technologies, USA) at a temperature of 200 °C, to make sure that the sample will be completely melted during analysis. The tests were carried out over a frequency range of 0.1–100 Hz at a constant amplitude of 5 %.

Differential scanning calorimetry. Melting temperature (T_m) and crystallization temperature (T_c) were measured using a differential scanning calorimeter (Discovery DSC25, TA Instrument, USA) under the N_2 atmosphere. The samples were heated from room temperature to 200 °C to remove their thermal history. Then, the samples were cooled to −80 °C, followed by a second heating step from −80 °C to 200 °C. The cooling and heating speeds were kept constant at 10 °C/min. The degree of crystallinity (X_c) of PVDF in the blends was determined, assuming a 100 % crystalline PVDF enthalpy of 104.6 J/g [38,39].

$$X_c\ (\%) = 100 \times \frac{\Delta H_m}{\Delta H^{\circ}_{m(100\%)} \times w_{PVDF}} \quad (3)$$

Thermogravimetric analysis. The thermal stability of PVDF/FKM/MGNR40 blends was determined by a thermogravimetric analyzer (TGA8000, PerkinElmer) set at a heating rate of 10 °C/min, from 25 °C to 600 °C under an N_2 atmosphere. The thermal characteristics of the samples are analyzed from thermogravimetric (TG) and thermogravimetric derivative (DTG) curves, depicted in Fig. S1 (Supporting information).

Oil resistance. TPV samples with dimensions of 5 x 5 × 1.5 mm^3 were immersed into different types of oil and solvent (i.e., toluene/isooctane mixture, diesel oil, and engine oil) for 72 h at room temperature. The oil resistance at high temperature of TPV in engine oil was also investigated at 125 °C for 22 h. The % change in mass of TPV was calculated by **Equation (4)** [40].

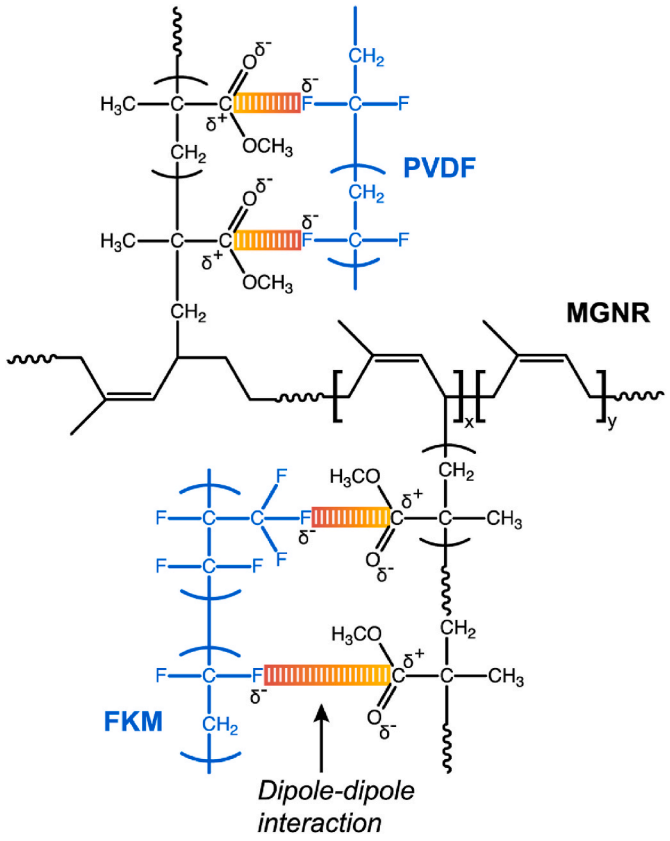

Fig. 4. Possible interfacial compatibilization and interactions between PVDF, FKM, and MGNR.

$$\%\ Change\ in\ mass = \frac{W_2 - W_1}{W_1} \times 100 \tag{4}$$

The volume swelling (q-1) was calculated using the following equation [41]:

$$q - 1 = \left(\frac{W_2}{W_1} - 1\right) \times \frac{\rho_2}{\rho_1} \tag{5}$$

where W_1 is the initial weight of the sample, W_2 is the weight of the swollen sample, and ρ_1 and ρ_2 are specific gravities or densities of solvent and sample, respectively.

Shape memory capability. The shape memory performance indicator measured in this work was the same as in our previous work [7]. The sample strips (40 mm × 6 mm x 1.5 mm) were first thermally bent into a U-shape by applying force and kept in hot water (~95 °C) for 10 min. The bent samples were moved into an ice bath (~5 °C). After 10 min, the temporary force was released, and the samples were maintained in the ice bath to obtain a temporary shape, which shows the fixity angle (θ_f). In the final step, the temporary shape was placed in a hot water bath (~95 °C) for 10 min to obtain the original shape, which shows a recovery angle (θ_r). The shape fixity ratio (R_f) and shape recovery ratio (R_r) were calculated using **Equations 6** and **7**, respectively [42].

$$R_f = \frac{180^\circ - \theta_f}{180^\circ} \times 100 \tag{6}$$

$$R_r = \frac{\theta_r - \theta_f}{180^\circ - \theta_f} \times 100 \tag{7}$$

Reprocessability of TPV. The TPV scraps were cut into small pieces and molded at similar conditions as for preparing TPV sheets (about 2 mm thick) using compression molding. Then dumbbell-shaped specimens were cut off from the recycled TPV sheets using ISO37 type II cutting die before assessing their mechanical properties by tensile testing machine.

3. Results and discussion

3.1. Mixing torque behavior

To evaluate the effects of blend composition and dynamic vulcanization of PVDF/FKM/MGNR blends, the mixing torque during the blending process was monitored and recorded. Torque-time evolution of the TPE and the TPV is shown in Fig. 1. The first peak was due to the melting of PVDF pellets. The mixing torque significantly increased again with the addition of FKM and MGNR into the mixing chamber. For TPEs, the torque gradually decreased to a plateau when all the polymers became homogenously blended. At the same time, the final mixing torque strongly depended on MGNR content in the TPE, where all **P0F4M**s showed the highest mixing torque and torque curves became relatively lower for the blends with higher FKM content. This is due to the higher viscosity of MGNR as compared to FKM (Fig. S2). The incorporation of curative (TPV) led to a remarkable increase in the mixing torque of the blend. This behavior confirmed that dynamic vulcanization occurred during the shearing action and blending of PVDF/FKM/MGNR TPVs. The dynamic vulcanization occurred through diamine cross-linking in rubber phases. The torque increment induced by dynamic vulcanization was evident for the TPV containing FKM because HMDC preferentially reacts with the FKM phase [43].

Fig. S3 shows the curing behaviors of FKM, FKM/MGNR, and MGNR with HMDC. The rheometer revealed that FKM can be fully vulcanized with a diamine curative [43,44]. According to our previous work [7], MGNR can be cross-linked with HMDC through ester groups of grafted PMMA and diamine, a so-called amidation reaction. However, the curing curve of MGNR with the diamine system was slightly increased (Fig. S3), indicating a slow cure rate of diamine-cured MGNR. Therefore, **P0F4M** TPVs showed a slight torque increment after dynamic vulcanization, indicating partly cross-linked MGNR with HMDC. Although the cure rate of MGNR with diamine was slow compared with FKM, the heat and shearing action generated during mixing can induce an amidation reaction between the diamine and ester group of MGNR. Interestingly, the final torques of ternary TPVs were higher than those of binary TPVs, indicating a possible cross-linking between FKM and MGNR (Fig. S4) and a synergistic effect boosted by three components.

3.2. Mechanical properties

To study the effects of blend ratio and blending procedure, the tensile responses of PVDF/FKM/MGNR40 blends with (TPV) and without diamine (TPE) were investigated, as shown in Fig. 2. As expected, the stress-strain behaviors of the blends varied according to the blend ratio and blending procedure. The TPE and TPV with a high PVDF proportion (**5P**) showed higher Young's moduli than the blend with a low PVDF fraction (i.e., **4P** and **3P**), which is a general trend for thermoplastic-elastomer blends. Also, in blends derived with the same PVDF/rubber ratio, Young's modulus, tensile strength, and elongation at break varied by FKM/MGNR ratios, indicating that grafted PMMA in MGNR and interfacial interactions play a role in the mechanical properties of the PVDF/FKM/MGNR based TPEs and TPVs. However, some compositions may not exhibit sufficient elongation at break (<50 %) to serve as thermoplastic elastomers.

The tensile properties of TPEs and TPVs are summarized in Fig. 3. It is evident that the tensile strength of both TPE and TPV decreased with rubber content, which was attributed to the higher amount of soft rubber in the blends. This is typical behavior for all TPEs and TPVs made from thermoplastic-rubber blends, as reported in the literature [21,45]. In addition, the blends with high rubber content exhibited higher elongations at break. This indicates that the mechanical properties of the PVDF/FKM/MGNR blends strongly depend on the blend proportions and morphology, which will be discussed later. Moreover, the binary

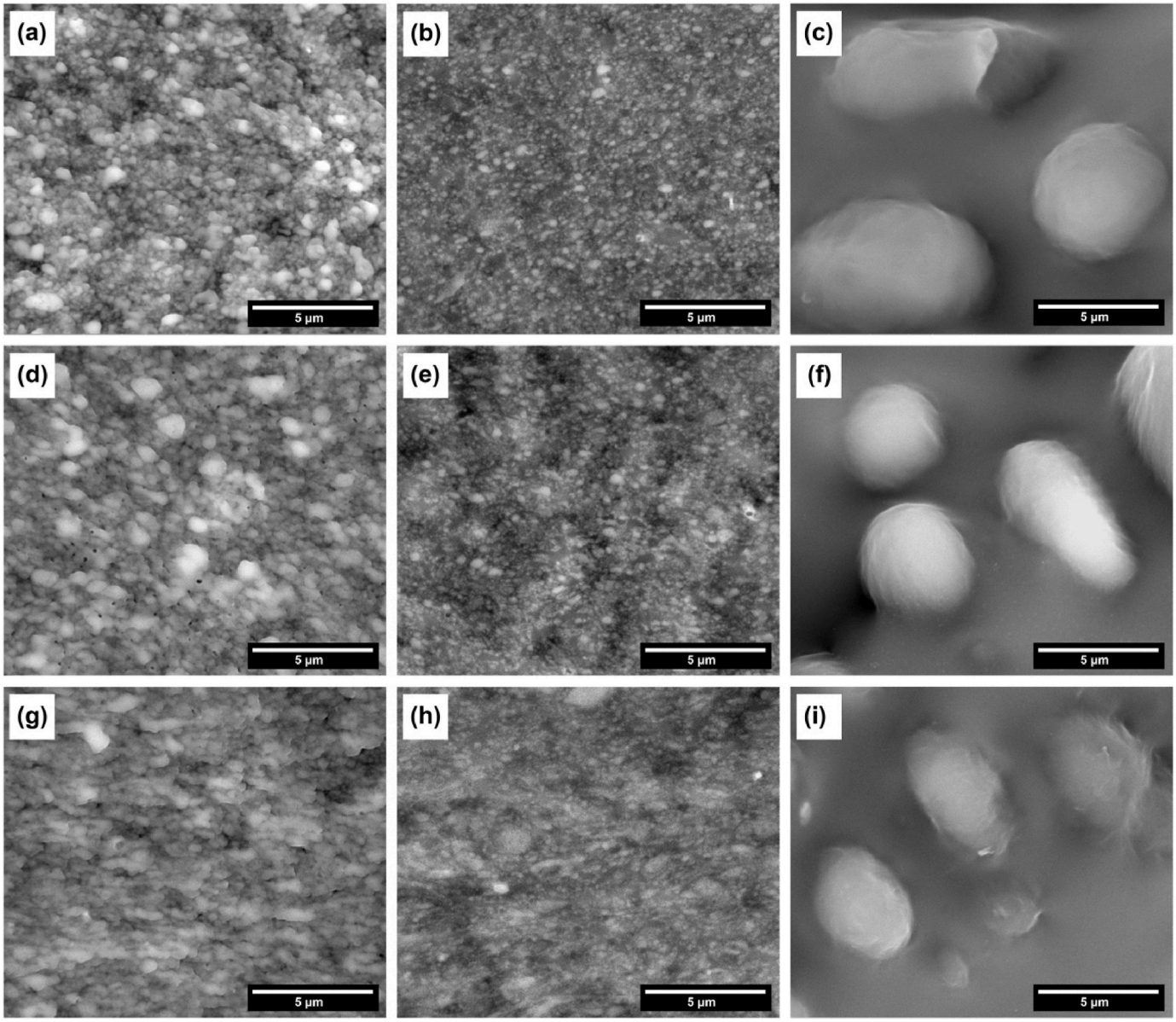

Fig. 5. SEM micrographs of PVDF/FKM/MGNR TPEs: (a) **5P0F4M**, (b) **5P2F2M**, (c) **5P4F0M**, (d) **4P0F4M**, (e) **4P2F2M** (f) **4P4F0M,** (g) **3P0F4M,** (h) **3P2F2M** and (i) **3P4F0M.**

PVDF/MGNR (**P0F4M**) blends without curative exhibited high tensile strength and low elongation at break because these blends contain glassy grafted PMMA domains from MGNR and crystalline regions of PVDF and could not be classified as TPEs. Hence, these blends exhibited higher tensile strength but were less flexible compared to the binary PVDF/FKM (**P4F0M**) blends without curative. At a given PVDF content, the tensile strength and elongation at break were improved for the TPE based on ternary PVDF/FKM/MGNR TPEs. This suggests that the glassy domain of MGNR could be diluted with FKM. It also suggests the possibility of interactions between blend components. As reported in our previous work, the improved mechanical properties are also due to the interfacial interactions between the grafted PMMA and PVDF [12]. Interestingly, after dynamic vulcanization, tensile strength improved significantly, whereas no significant change in elongation at break was observed (Fig. S5). This was attributed to the cross-linking of rubber phases in PVDF/FKM/MGNR blends, resulting in improved mechanical properties. Importantly, the tensile strength of **P4F0M** TPVs was significantly higher than that of **P4F0M** TPEs because FKM domains were partially cross-linked by dynamic vulcanization. For example, the tensile strength increased from 6.5 MPa for **5P4F0M** TPE to 19.8 MPa for **5P4F0M** TPV, which is a 3-fold increase induced by dynamic vulcanization.

Interestingly, the mechanical properties of both the TPEs and the TPVs made from ternary blends were significantly higher than those of the binary blends. This indicates a synergistic effect of the three components in these ternary blends. The PVDF and FKM are fluorine-containing polymers. PVDF is a VDF homopolymer, and FKM is a VDF-HFP copolymer. The fluorinated polymer is compatible with the acrylate polymer due to dipole-dipole interactions between carbonyl (C=O) and fluorine groups [46–48]. It was found that the PVDF is partially compatible with poly(methyl methacrylate)-grafted-natural rubber (MGNR), and the mechanical properties of PVDF/MGNR blends were significantly better than those of PVDF/NR blends [12]. As a result, carbonyl groups in MGNR are also expected to promote strong interactions with PVDF and FKM. A schematic illustration of possible dipole-dipole interactions in PVDF-MGNR-FKM is shown in Fig. 4. Furthermore, Fig. 3 also shows that ternary TPEs with high MGNR proportion (i.e., **P1F3M** and **P2F2M**) exhibited better mechanical

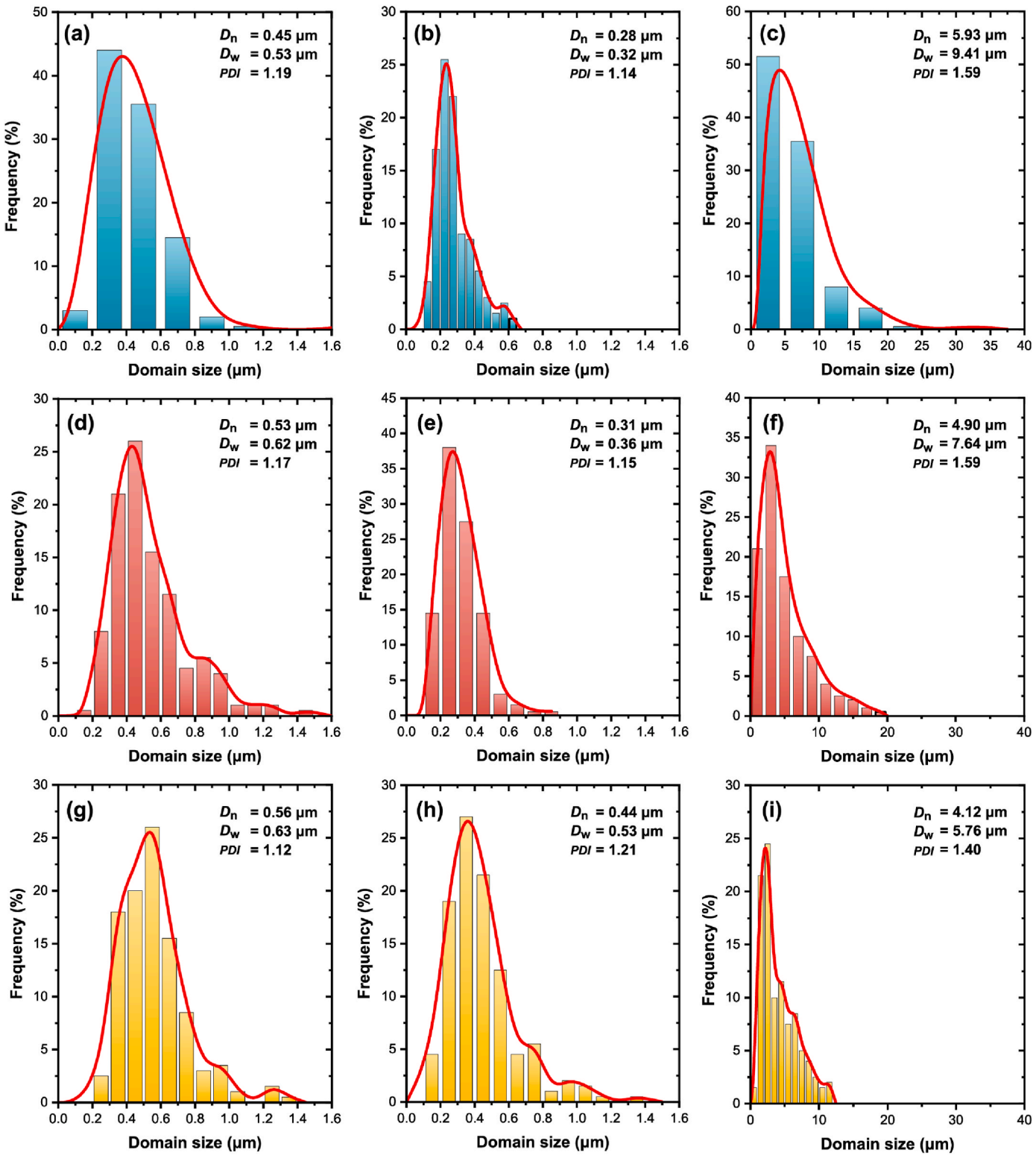

Fig. 6. Domain size distribution of the PVDF/FKM/MGNR TPEs: (a) **5P0F4M**, (b) **5P2F2M**, (c) **5P4F0M**, (d) **4P0F4M**, (e) **4P2F2M** (f) **4P4F0M,** (g) **3P0F4M,** (h) **3P2F2M** and (i) **3P4F0M.** The smooth red line may illustrate the overall shape of the distribution more clearly than the histogram. (For interpretation of the references to color in this figure legend, the reader is referred to the Web version of this article.)

properties than TPEs with high FKM proportion (i.e., **P3F1M**). In contrast, the ternary TPVs with high FKM proportion (i.e., **P2F2M** and **P3F1M**) exhibited better mechanical properties than TPVs with high MGNR proportion (i.e., **P1F3M**). This can be explained by the fact that FKM rubber is preferentially cured by HMDC due to reactive VDF/HFP dyads in FKM backbones [49]. At the same time, grafted PMMA in MGNR domains can provide cross-linking sites for diamine through an amidation reaction between the ester group on MGNR and diamine [7]. Consequently, the MGNR phase was partly vulcanized with FKM rubber in the ternary blends (Fig. S4), as discussed earlier. As a result,

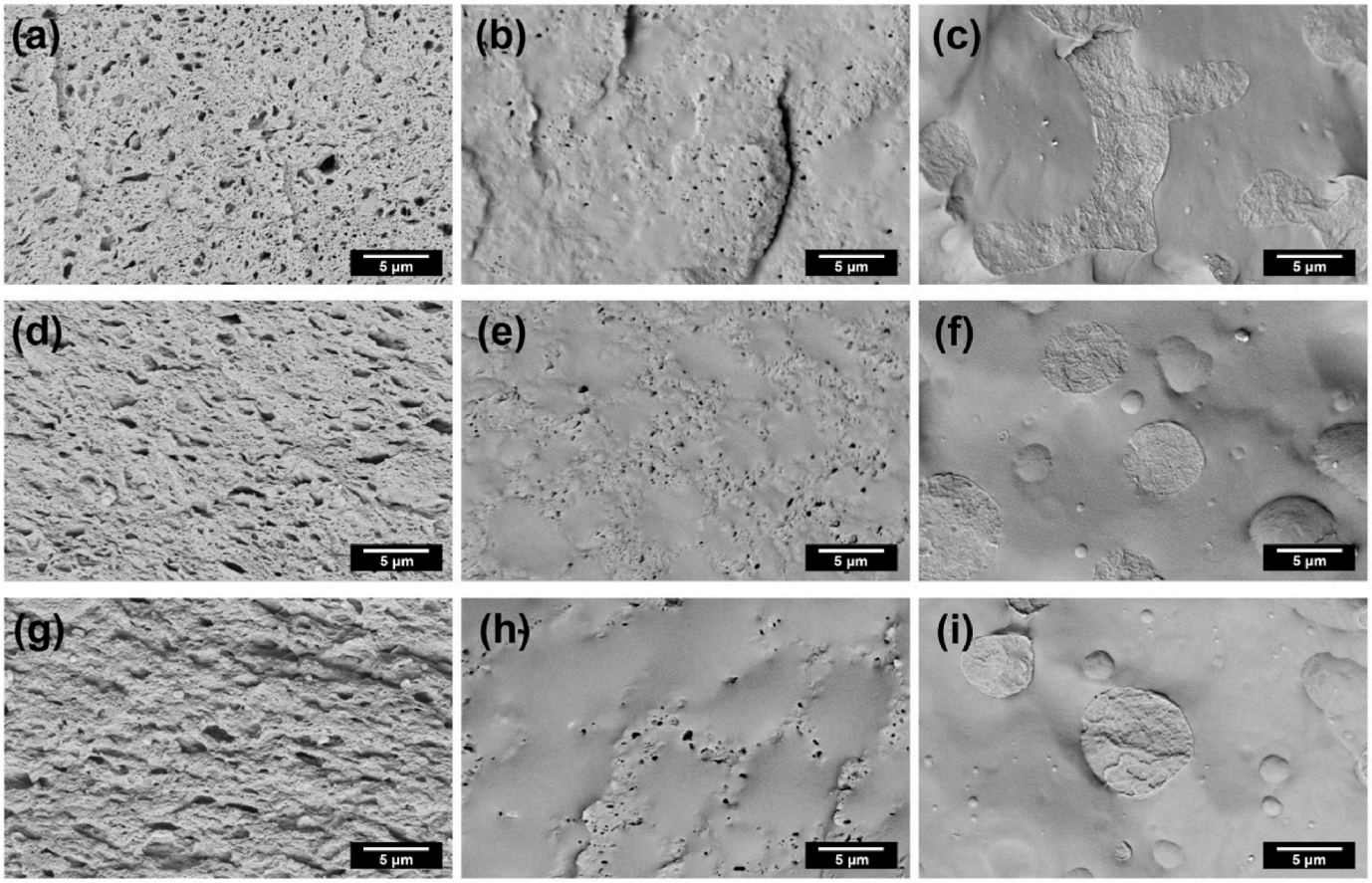

Fig. 7. SEM micrographs of etched PVDF/FKM/MGNR TPEs: (a) **5P0F4M**, (b) **5P2F2M**, (c) **5P4F0M**, (d) **4P0F4M**, (e) **4P2F2M** (f) **4P4F0M,** (g) **3P0F4M,** (h) **3P2F2M,** and (i) **3P4F0M.** These SEM images were taken at a magnification of 15,000x.

dipole-dipole interactions and co-crosslinking between FKM and MGNR phases can boost the physical properties of ternary TPV based on PVDF/FKM/MGNR blends.

3.3. Morphology

Morphology plays a critical role in determining the properties and performance of thermoplastic elastomeric materials (TPE and TPV) made from thermoplastic-rubber blends. In the context of blending modified NR with PVDF and FKM, a fundamental understanding of phase morphological structures of TPE and TPV made from binary and ternary blends is essential to tailor the final material properties for a specific application. In order to assess the evolution of phase morphology of the binary and ternary blends, the bright spots in SEM were measured and analyzed, and these are referred to as "domains" in the blends. As shown in Fig. 5, SEM micrographs clearly show that the continuous-dispersed phase morphology and domain sizes are strongly dominated by blend ratio and blend components. Fine dispersions were observed for **P0F4M** (Fig. 5(a), (d), and (g)) and **P2F2M** TPEs (Fig. 5(b), (e), and (h)), while **P4F0M** TPEs showed coarse domains in the blend (Fig. 5(c), (f), and (i)). SEM micrographs of TPEs at a lower magnification are shown in Fig. S6. The broad domain size distribution of **P4F0M** TPEs varied in the range of 1.5–20.0 μm. In contrast, the size of a domain diameter in **P0F4M** and **P2F2M** TPEs is consistently smaller than 1.5 μm, as summarized in Fig. 6. For binary PVDF/FKM (**P4F0M**) blends without curative, the large bright phases (domains) with a number-average diameter size of 4.0–6.0 μm are clearly dispersed in the dark phase.

The morphology in a polymer blend can be influenced by various factors, including the viscosities of blend components, blend composition, processing techniques, compatibilization technique, and interfacial interactions between the components [50–52]. The absolute value of complex viscosity (η^*) of each blend component at 200 °C is shown in Fig. S7, and the viscosity ratio is summarized in Table S1. By varying the viscosity ratio of blend components, the influences on phase morphology, domain dispersion, and interfacial interactions in binary and ternary blends were investigated. It was found that the η^* of PVDF and MGNR were higher than that of FKM, and the viscosity ratio varied between 0.21 and 1.47, which certainly plays a role in phase morphology. For example, the binary FKM/PVDF TPEs made with 50 wt % (**5P4F0M**), 60 wt% (**4P4F0M**), and 70 wt% (**3P4F0M**) of FKM had a large volume of FKM and low viscosity ratio ($\eta_{FKM}/\eta_{PVDF} = 0.31$). Thus, high-viscosity PVDF can be broken up by shear forces during melt mixing and could be encapsulated by the FKM phase [50,51]. However, with the low viscosity of FKM and the large difference in viscosity of FKM and PVDF, the FKM matrix phase cannot break up PVDF effectively. However, PVDF and FKM are both fluorinated polymers with similar chemical structures. According to this viscosity ratio and mixing parameter, the PVDF phase was less deformed, and large dispersed PVDF domains ($D_n = 4.0–6.0$ μm) were observed in the FKM matrix, as shown in Fig. 6(c), (f), and (i). Therefore, the brighter and darker regions in binary FKM/PVDF blends are likely to correspond to PVDF and FKM phases, respectively.

In contrast, the binary MGNR/PVDF (**P0F4M**) TPEs showed an abrupt reduction in dispersed domain size as compared to **P4F0M** TPEs. For example, the domain size was significantly reduced from 4.9 μm for **4P4F0M** TPEs to 0.53 μm for **4P0F4M** TPEs, which is ten times smaller than in binary FKM/MGNR blends. This can be explained by the fact that the viscosity ratio of the MGNR/PVDF system ($\eta_{MGNR}/\eta_{PVDF} = 1.47$) was almost 5-fold higher than in the FKM/PVDF system ($\eta_{FKM}/\eta_{PVDF} = 0.31$).

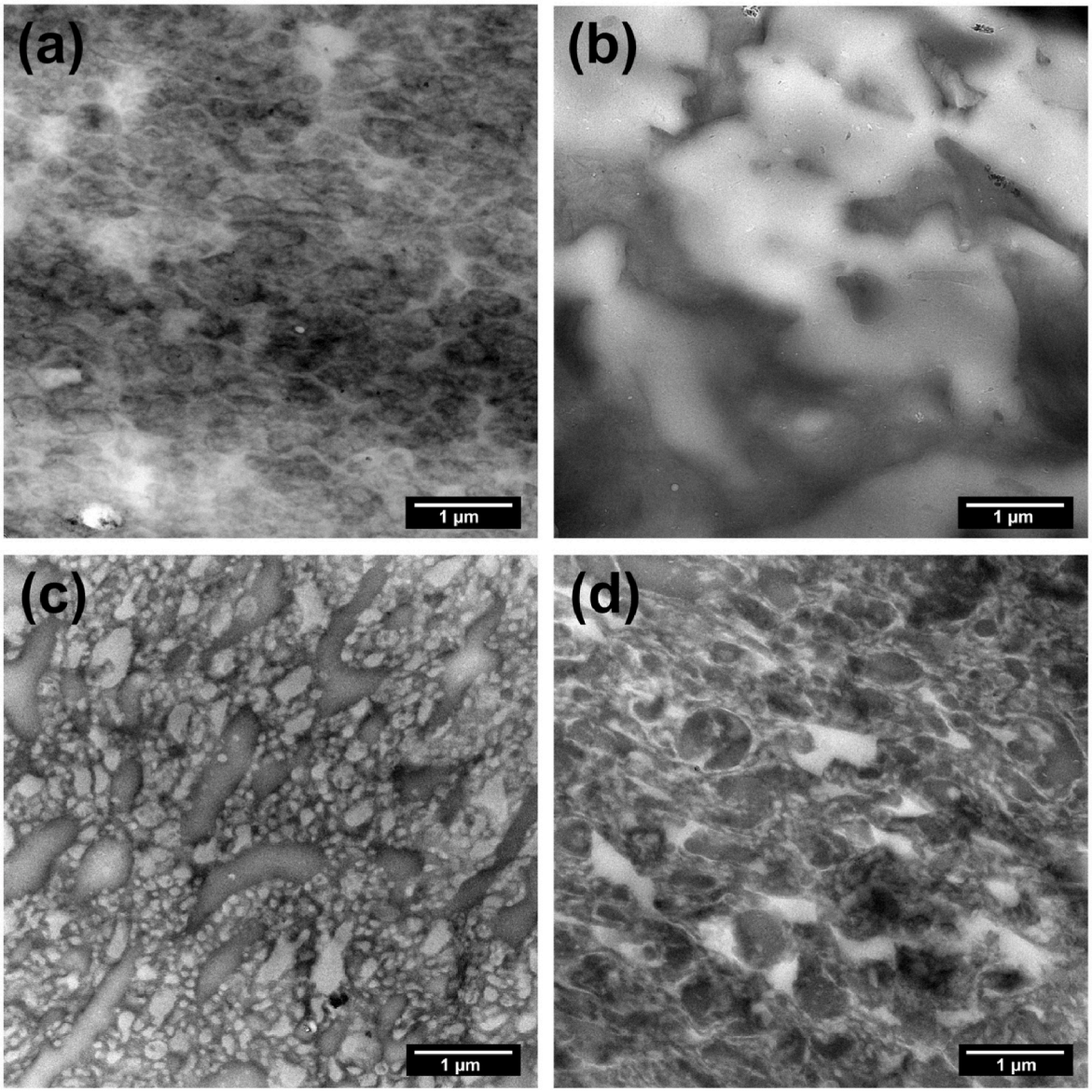

Fig. 8. TEM micrographs of PVDF/FKM/MGNR blends: (a) **4P0F4M** TPV, (b) **4P4F0M** TPV, (c) **4P2F2M** TPE, and (d) **4P2F2M** TPV. All micrographs were taken at a magnification of 11,000x.

Therefore, the viscosity ratio is critical for achieving a smaller domain size [50]. On the other hand, C=O groups of MGNR also facilitate dipole-dipole interactions with C-F groups in PVDF. In this blend system, PVDF exhibited lower viscosity than MGNR. As a result, the PVDF phase tends to form a continuous phase and break up the MGNR phase. However, the bright and dark regions in SEM micrographs of MGNR/PVDF TPEs are likely due to MGNR and PVDF. This differs from SEM micrographs of FKM/PVDF TPEs, where PVDF is the bright phase. The difference can be correlated with the electron density of each component, which can influence phase morphology. Polymers with similar electron densities tend to have stronger interactions between the blend phases, resulting in better miscibility and compatibility, whereas blend components with very different electron densities may have weak interactions, resulting in poor miscibility and compatibility. The morphology observation was also confirmed by SEM micrographs of etched samples, as shown in Fig. 7. The MGNR phase was selectively extracted with toluene for 3 days. It can be observed that **P0F4M** TPEs showed matrix-droplet morphology. The holes displayed in **P0F4M** TPEs represent the MGNR phase after solvent treatment, indicating the dispersion of MGNR in the continuous PVDF matrix. In contrast, the hole-like structures are absent in **P4F0M** TPEs (Fig. 7(c), (f), and (i)) because toluene cannot remove FKM and PVDF regions. Meanwhile, the rough surfaces in SEM represent the PVDF phase, and the smooth surfaces represent the FKM phase due to the crystalline component in PVDF and the amorphous nature of FKM. This confirms that PVDF in **P4F0M** TPEs was dispersed in FKM, as discussed earlier. Interestingly, the addition of third components alters the phase structure and distribution in the blend system. The phase morphology seems to be improved for ternary TPE **(P2F2M)**, as indicated by the smaller bright spots and the smaller holes in (Fig. 5b, e, 5h, 7b, 7e, and 7h). The improved phase morphology observed in ternary blends is attributed to possible synergistic interactions between the three components, resulting in finer domain dispersion and improved mechanical properties. Surprisingly, **P0F4M** blends showed a smaller domain size than **P4F0M** blends, whereas ternary **P2F2M** blends showed the smallest domain size. For example, the domain size was significantly reduced from 4.9 μm for 4P4F0M to 0.53 μm for **4P0F4M** and to 0.31 μm for **4P2F2M**, as shown in Fig. 6. The finer phase morphology of the ternary blend can be correlated with compatibility, intramolecular interactions, and overall thermodynamic behavior. The strong dipole-dipole interactions

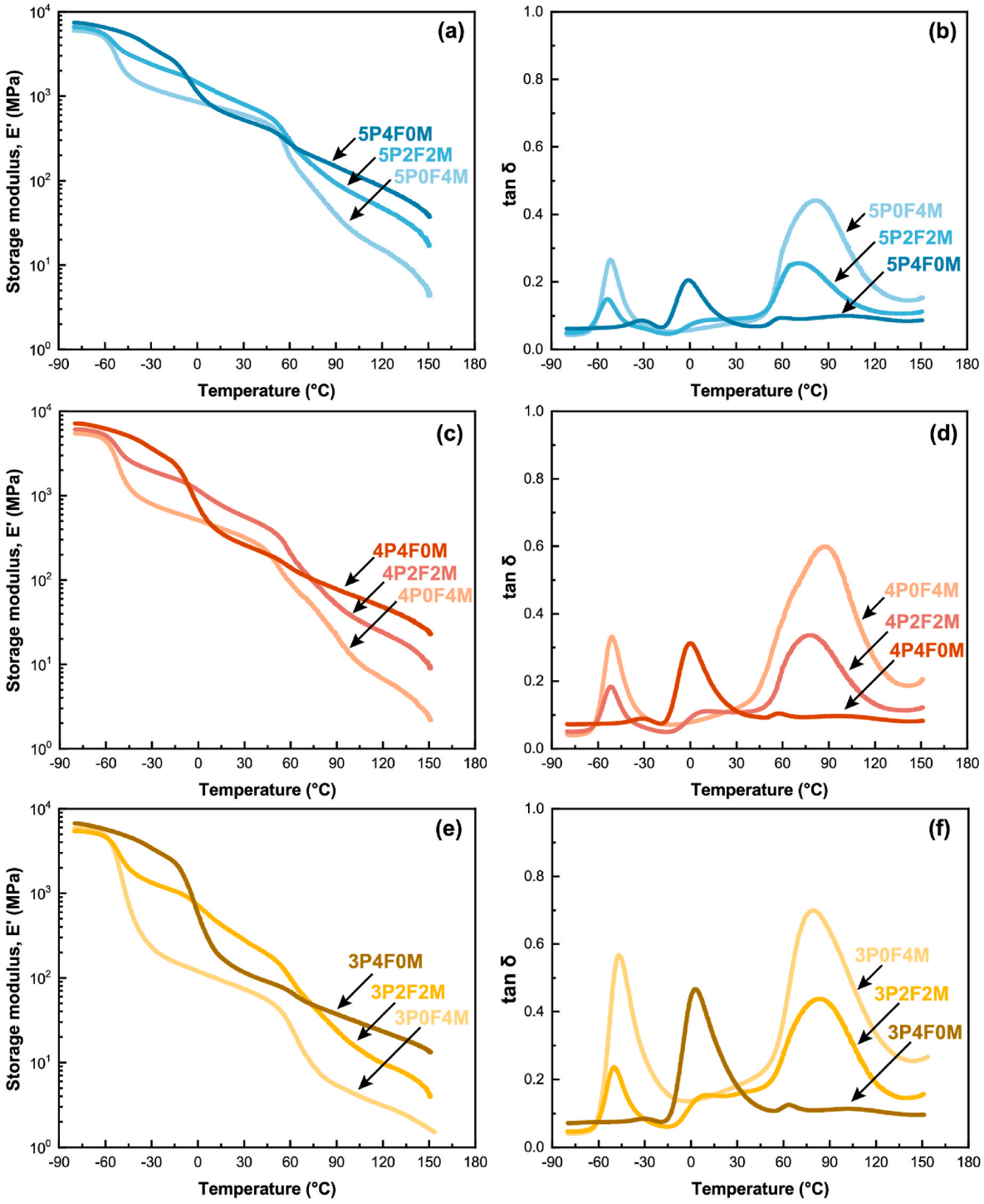

Fig. 9. (a, c, e) Storage modulus (E'), and (b, d, f) tan δ versus temperature of PVDF/FKM/MGNR40 blends with different PVDF/rubber ratios: (a, b) 50/50 wt% (**5P**), (c, d) 40/60 wt% (**4P**), and (e, f) 30/70 wt% (**3P**).

between the C=O group of MGNR and the C-F group of both PVDF and FKM contributed to a reduction in the interfacial tension in the ternary blend system. This tends to stabilize the domains, which can lead to improved microstructure and mechanical performance of the blends.

The SEM micrographs of TPVs also showed improved morphology for ternary TPV (Fig. S8). Although the phase boundary observed by SEM was blurred due to compatibility between the three phases, all SEM micrographs showed a similar tendency for morphology improvement. Subsequently, the phase morphology of the TPVs was further evaluated by TEM imaging, as shown in Figs. 8 and S9. The morphologies of the ternary blends were significantly better than those in the binary blends. At the same time, the binary **4P0F4M** TPV showed finer phase dispersion than **4P4F0M** TPV, correlating well with SEM results. In literature, TEM imaging revealed that PVDF and FKM usually exhibited as dark and bright regions, respectively [36,53,54]. Also, according to our previous work, PVDF also showed darker regions than MGNR regions [12] and ENR [32]. Nevertheless, it is worth noting that color appearance also depends on component pairs in the blend. Consequently, it is assumed that the dark, gray, and bright regions in the TEM micrographs correspond to PVDF, MGNR, and FKM, respectively. The binary **4P0F4M** TPV

Table 2
Storage modulus and T_g obtained from DMA analysis.

Sample	E'@30 °C (MPa)	T_g (°C)			
		NR	PVDF	FKM	Grafted PMMA
PVDF	1800		−32.3		
FKM	3.0			2.7	
MGNR	215	−51.0			117.8
5P0F4M TPV	600	−51.5	(–)		81.8
5P2F2M TPV	860	−53.4	(–)	5.5	70.7
5P4F0M TPV	526		−31.0	−1.0	
4P0F4M TPV	325	−51.0	(–)		87.6
4P2F2M TPV	578	−51.1	(–)	9.9	78.0
4P4F0M TPV	260		−31.0	0.1	
3P0F4M TPV	72	−46.3	(–)		79.2
3P2F2M TPV	290	−49.8	(–)	11.2	81.3
3P4F0M TPV	115		−30.0	2.9	

Dash (−) means that the T_g could not able to be determined from DMA curves.

(Figs. 8a and S9a) exhibited small phase sizes, and gray regions were partially located in dark regions because of the dipole-dipole interaction between grafted PMMA and PVDF. This is correlated well with our previous work [12] in which carbonyl groups in MGNR improved interfacial interaction between PVDF and MGNR. Notably, the phase morphology of diamine-cured TPV was different from phenolic-cured TPV, indicating that the choice of the cross-linking system affects the microstructure of TPV. In contrast, the binary TPV based on the PVDF/FKM blend (**4P4F0M**) showed large FKM particles dispersed in PVDF (Figs. 8b and S9b). The blend ratio of 40/60/0 wt% led to an incomplete phase inversion during mixing, resulting in a disruption of the droplet-island structure of TPV. Therefore, the rubber-rich cases of TPV could have large cross-linked rubber particles and partly co-continuous morphology [12,55].

As shown in Figs. 8c and S9c, a fine morphology was observed in **4P2F2M** TPE. In this case, it seems that there was no particular matrix phase, and the three phases were co-dispersed in the blends. Particle size distribution was in the range of 70–300 nm, with most particles smaller than 150 nm. As this blend ratio is dynamically cured with diamine (**4P2F2M** TPV), in Figs. 8d and S9d, it is likely to exhibit improved morphology due to cross-linking of rubber phases during melt mixing. The bright regions (FKM) were reduced after dynamic vulcanization, which might be due to the compatibilization and co-vulcanization of FKM with MGNR. At the same time, some MGNR phases (gray regions) were located at the boundary of FKM and PVDF, as shown in a TEM image at higher magnification (Fig. S9d). Combining strong dipole-dipole interactions between PVDF-MGNR-FKM (Fig. 4) and dynamic vulcanization between FKM and MGNR contributed notably improved mechanical properties and phase morphology.

AFM was also used to characterize phase structure in PVDF/FKM/MGNR TPVs, as shown in Fig. S10. **4P4F0M** TPV (Fig. S10c) clearly showed phase separation with coarse co-continuous morphology where the light regions represent high modulus PVDF phase and dark regions represent low modulus FKM phase. The coarse morphology of **4P4F0M** TPV was similar in the TEM micrograph (Fig. 8(d)), demonstrating incomplete phase inversion at this blend ratio. In contrast, the phase separation in the AFM images of **4P0F4M** and **4P2F2M** TPVs (Figs. S10a and S10b) was not clear, and those blends are likely homogenous and have improved interfacial interaction through dipole-dipole interactions (TPE and TPV) and dynamic vulcanization (TPV). It is worth noting that the unclear phase separation in AFM might be due to a very small domain size (<500 nm) in **4P0F4M** and **4P2F2M** TPVs, as observed in Figs. 8 and S9.

3.4. Dynamic mechanical analysis (DMA) and rheological behavior

The compatibility in the blends regulates phase dispersion by physical and chemical interactions, and significantly impacts the mechanical performance, viscoelastic properties, and thermal properties. Therefore, dynamic mechanical analysis (DMA) and rheological determinations were run to assess the improvement of compatibility and viscous flow of the PVDF/FKM/MGNR40 blends. The DMA analysis of pure PVDF, FKM, and MGNR40 is shown in Fig. S11, whereas the storage modulus (E') and tan δ curves of the PVDF/FKM/MGNR40 TPVs are shown in Fig. 9. The dynamic mechanical parameters are summarized in Table 2. The abrupt decrease of storage modulus and the presence of tan δ peak are associated with glass transition temperature (T_g) or molecular relaxation of the materials. The tan δ curve shows a strong peak at −32 °C for neat PVDF. This relaxation at a lower temperature (−32 °C) of neat PVDF is known as β or α_a relaxation, and it corresponds to segmental motions in the amorphous regions or T_g of PVDF. The PVDF also showed an additional peak at the higher 75 °C temperature, which is related to α relaxation. This is because of segmental motions in the crystalline region of PVDF [56,57]. The DMA curve of FKM showed only a single relaxation at 2.7 °C due to T_g of FKM rubber. Meanwhile, MGNR40 showed two strong tan δ peaks at temperatures of −50 °C and 117.8 °C. The lower temperature is due to T_g of the NR main chains, whereas the higher temperature is mainly attributed to the T_g of the grafted PMMA domain and PMMA homopolymer in MGNR.

Interestingly, the reduction in magnitude of E' was most dependent on the blend ratio of components. The decline in E' at different regions is associated with the molecular relaxation of each component. This relaxation shows in the tan δ peaks, as described earlier. As shown in Fig. 9, the binary blends with 100 % MGNR fraction (i.e., **P0F4M** TPV) and ternary blends (i.e., **P2F2M** TPV) exhibited a clear abrupt drop of E' in the first region (−80 to −30 °C) due to the glass transition of the NR backbone and low-temperature flexibility of the blends. Above −30 °C, E' of binary **P4F0M** TPV significantly dropped due to the relaxation of PVDF and FKM phases. Importantly, **P2F2M** TPV showed the highest E' compared to **P0F4M** and **P4F0M** TPVs, as summarized in Table 2. This indicates the synergistic effect in a ternary blend of PVDF, FKM, and MGNR40. At the same time, the three components improved viscoelastic properties and compatibility in the blends due to physical and chemical interactions between the three phases. Above 60 °C, the dramatic decrease in E' was noticeable again for **P0F4M** and **P2F2M** TPVs due to softening of grafted PMMA and crystalline PVDF. Hence, E' was remarkably reduced for those blends.

All **P0F4M** blends display two noticeable drops of E' at −60 °C and 70 °C, corresponding to the glass transition temperatures (T_gs) of natural rubber and NR-g-PMMA domains. At the same time, it is seen that all **P4F0M** also displays two T_gs, which correspond to T_g of PVDF (−35 °C) and of FKM (0 °C). However, the T_g of PVDF cannot be observed in **P0F4M** blends because of small β-relaxation and low PVDF proportion in the blends. Also, β -relaxation of PVDF overlapped with the T_g of NR. The ternary blends (i.e., **P2F2M**) are expected to show four tan δ peaks associated with NR, grafted PMMA, PVDF, and FKM. However, all **P2F2M** samples displayed only tan δ peaks of NR, FKM, and grafted PMMA because the T_g of PVDF was merged entirely with the T_g of NR, as mentioned earlier. The maximum peaks of tan δ of each component had shifted toward each other, as summarized in Table 2. It can be observed that the maximum peak of tan δ (T_g) of grafted PMMA shifted to a lower temperature, and T_g of FKM shifted to a higher temperature, as compared to neat NR-g-PMMA and FKM, respectively. This phenomenon was attributed to improved interfacial interaction and miscibility between these blend components [12]. A plausible interaction in this system is proposed in Fig. 4. Fig. S12 shows the DMA curves of ternary TPEs, and TPVs based on PVDF/FKM/MGNR blends. It is seen that E' of TPV was slightly higher than that of TPE. Meanwhile, T_gs of each region in TPV were shifted toward each other. This result indicates the effect of reactive blend induced by dynamic vulcanization and synergism in the ternary TPV, which led to improved compatibility, viscoelastic properties and phase morphology, as discussed earlier.

To study viscoelastic behavior at elevated temperatures of the

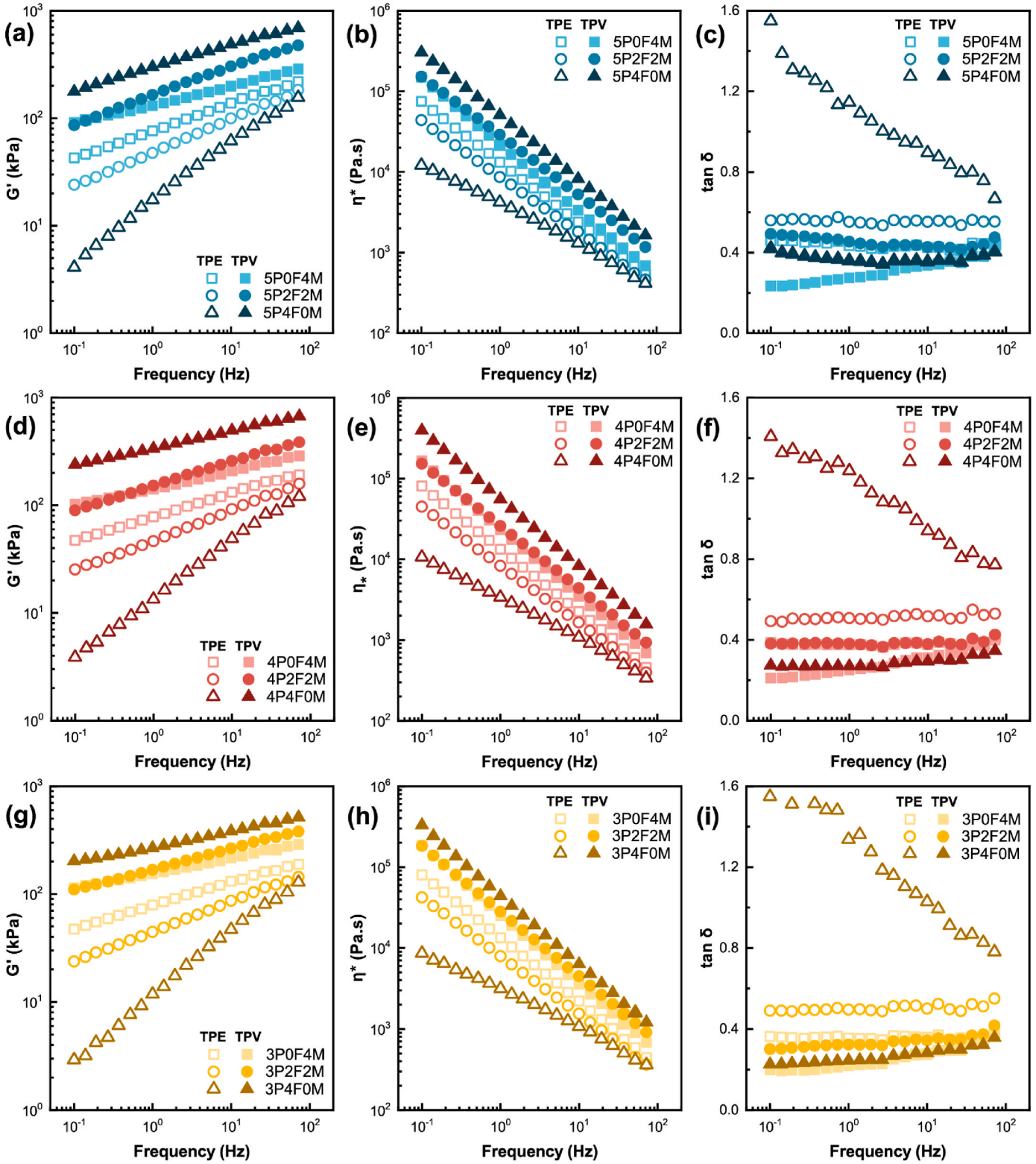

Fig. 10. Rheological properties of PVDF/FKM/MGNR TPEs and TPVs with different blend ratios: (a–c) 50 wt% PVDF (**5P**), (d–f) 40 wt% PVDF (**4P**), and (g–i) 30 wt% PVDF (**3P**).

blends, the shear modulus, complex viscosity, and tan δ were evaluated to assess the influence of dynamic vulcanization and blend proportions on the viscous flow. Fig. 10 shows the frequency dependence of storage modulus (G'), complex viscosity (η^*), and loss tangent (tan δ) of PVDF/FKM/MGNR blends. At the given blend ratio, **P4F0M** TPE exhibited lower G' and η^* than **P0F4M** TPE because FKM rubber has lower G' and η^* than MGNR and PVDF, as shown in Fig. S7. Therefore, the melt rheology of PVDF/FKM TPE was significantly improved for ternary blend PVDF/FKM/MGNR TPEs. After dynamic vulcanization, the G' and η^* of all TPVs were significantly increased, whereas tan δ was reduced. This suggests that dynamic vulcanization during melt mixing could enhance molecular chain restriction and improve elasticity, confirming

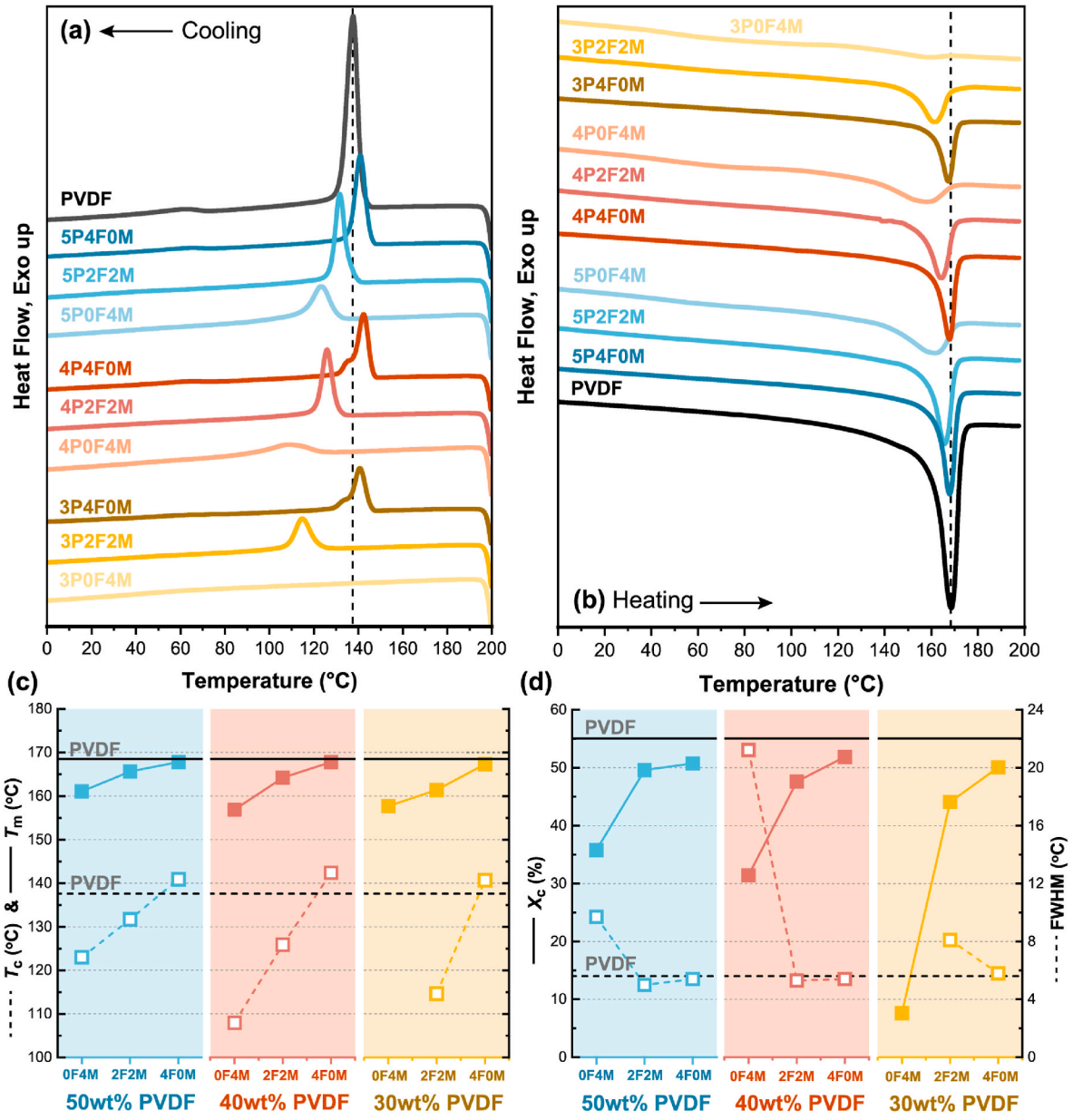

Fig. 11. (a) DSC cooling curves and (b) DSC heating curves for PVDF/FKM/MGNR TPV with different blend proportions. (c) Crystallization temperature and melting temperature of PVDF in PVDF/FKM/MGNR TPV. (d) Crystallinity percentage of PVDF and FWHM based on the crystalline peak.

the diamine cure of rubber phases. Interestingly, **P4F0M** blends display exceptionally improved viscoelastic parameters after dynamic vulcanization, as G' and η^* reached their highest values, and a significant reduction of tan δ was observed. This can be explained by the fact that FKM domains in PVDF/FKM TPVs were fully cross-linked by diamine. However, G' and η^* of TPVs were reduced by the MGNR proportion because diamine-cured FKM was partly replaced with diamine-cured MGNR in which diamine curative (HMDC) vulcanization rate and efficiency were lower than in FKM. Therefore, the melt strength and viscoelastic behavior of **P2F2M** and **P0F4M** TPVs were lower than those of **P4F0M** TPVs. This correlated well with the E' trends from DMA analysis at elevated temperatures (Fig. 9). In addition, the results in Fig. 10 also confirm that MGNR in **P0F4M** TPVs was partly crosslinked with diamine curative, as G' and η^* of **P0F4M** TPVs were higher and tan δ lower than **P0F4M** TPEs. According to the rheological behavior result, the flow characteristics were compromised and can be manipulated with three components of the blend and cross-linking network in the rubber phase.

3.5. *Differential scanning calorimetry (DSC)*

PVDF is a semi-crystalline polymer, while FKM and MGNR are amorphous polymers. The crystallinity of PVDF phase is strongly dependent on miscibility and interfacial interactions. Fig. 11(a) and (b) presents the cooling and melting behavior of PVDF/FKM/MGNR TPV, respectively. Pure PVDF showed an exothermic peak at 137.6 °C, which is the crystallization temperature (T_c). During the second heating, the endothermic event (168.5 °C) can be assigned to melting temperature (T_m). The PVDF binary blends with FKM (**P4F0M**), MGNR (**P0F4M**), or ternary blend (**P2F2M**) caused changes in both crystalline and melting temperatures. The details of DSC results are summarized in Fig. 11(c) and (d). All **P4F0M** TPVs exhibited slightly higher T_c than neat PVDF, while T_cs of **P2F2M** and **P0F4M** TPVs were significantly reduced compared to PVDF. Meanwhile, T_m tended to be reduced for all TPVs. As shown in Fig. 11(c) and (d), the T_c and T_m of PVDF in **P0F4M** TPVs were significantly lower than **P4F0M** and **P2F2M** TPVs, and both exothermic and endothermic peaks became broadened with increasing MGNR

Table 3
Thermal characteristics of PVDF, FKM, MGNR, and the PVDF/FKM/MGNR TPV with different blend ratios.

Sample	$T_{5\%}$ [a] (°C)	$T_{30\ \%}$ [b] (°C)	$T_{50\ \%}$ [c] (°C)	T_{HRI} [d] (°C)	T_{max1} [e] (°C)	T_{max2} [f] (°C)	T_f [g] (°C)	R_w [h] (%)
PVDF	459.4	477.9	488.1	230.5	-	477.7	493.1	35.02
FKM	453.6	469.5	475.0	226.9	-	476.2	486.3	0.64
MGNR	294.4	380.3	390.4	169.5	392.5	–	412.9	1.36
5P0F4M	308.7	391.0	420.2	175.5	398.8	–	453.8	24.9
5P2F2M	337.4	437.8	494.2	194.8	395.0	498.9	515.9	32.4
5P4F0M	401.8	481.3	500.1	220.3	–	491.3	513.4	30.2
4P0F4M	296.0	382.1	409.9	170.4	394.5	–	451.3	31.0
4P2F2M	333.8	424.1	491.7	190.1	400.4	500.3	523.8	28.4
4P4F0M	399.5	482.7	499.5	220.2	–	494.4	513.4	20.8
3P0F4M	299.7	380.2	404.5	170.5	390.7	–	449.8	17.9
3P2F2M	332.5	408.4	468.6	185.2	394.5	483.8	510.5	29.9
3P4F0M	403.5	486.0	504.7	222.0	–	498.5	526.1	26.7

[a] Temperature at 5% weight loss.
[b] Temperature at 30% weight loss.
[c] Temperature at 50% weight loss.
[d] The heat-resistance index; $T_{HRI} = 0.49 \times [T_{5\%} + 0.6 \times (T_{30\%} - T_{5\%})]$ [66].
[e] Temperature at the maximum decomposition rate of MGNR phase.
[f] TTemperature at the maximum decomposition rate of PVDF or FKM phases.
[g] Final decomposition temperature.
[h] Residual weight retention at 600 °C.

content due to the interphase compatibility. Decreases in T_c and T_m of PVDF were also observed by other researchers [58,59]. According to our previous work [12], the PVDF and MGNR are more compatible when grafted PMMA content and blend ratio are increased, resulting in a reduction in T_c and T_m of PVDF. According to the DSC results, the grafted PMMA chains enhance intermolecular interactions with PVDF through dipole-dipole interactions [12,60]. In addition, as shown in Fig. 11(d), the full width at half-maximum (FWHM) of the exothermic peak increased with MGNR content, indicating that MGNR domains and interfacial interactions impede the growth of PVDF crystals [59].

Based on the melting peaks, the crystallinity can be estimated from the enthalpy of melting by using **Equation (3)**. As shown in Fig. 11(d), the crystallinity (X_c) in TPV was remarkably reduced with increasing MGNR proportion and with decreasing PVDF content, especially in the PVDF/MGNR blends (**P0F4M**) and **3P** series. For example, the melting peak in **3P0F4M** TPV almost disappeared. This was attributed to the inhibition of crystallization in the PVDF phase by strong interactions and good miscibility between PVDF and MGNR [12,61]. The low crystallinity of PVDF/acrylate polymer blend has been widely discussed in the literature [62,63]. Although FKM is a fluorinated elastomer containing VDF copolymer, which is similar to PVDF, the incorporation of FKM could not reduce X_c as much as MGNR. This reveals that the interactions between carbonyl groups (C=O) of grafted PMMA in MGNR and CF_2 groups of PVDF are stronger than the interaction between PVDF and FKM. Hence, the crystallization ability of the thermoplastic domain was dramatically reduced by the presence of a well-compatible polymer pair [12,64]. Meanwhile, the large domains of the FKM phase in the blends and FKM chains do not dilute the amorphous phase of PVDF, so they cannot be involved in the crystallization process of PVDF.

3.6. Thermogravimetric analysis (TGA)

The thermal stability of neat polymers and PVDF/FKM/MGNR blends has also been investigated by thermogravimetric analyses, as shown in Figs. S13 and 12, respectively. The thermal characteristics of the samples are reported in Table 3. All neat polymers showed a single main decomposition step associated with their main chain degradation. It is obvious that the initial degradation temperature ($T_{5\%}$) and decomposition temperature of the PVDF and FKM were much better than those of MGNR, occurring at the temperatures 478 °C, 476 °C, and 392 °C, respectively. The PVDF and FKM are fluorine-containing polymers, which can provide much better thermostability and chemical resistance than polyolefin because bond energy and strength of the C-F bond are higher than those of C-C and C-H bonds [65]. As shown in Fig. 12, it is evident from weight loss and DTG curves that all **P0F4M** and **P4F0M** TPVs display single-step degradation behavior. In contrast, all **P2F2M** TPVs exhibited double-step degradation behavior. The two DTG peaks of **P2F2M** TPV are mainly attributed to crosslinked networks in TPV. In comparison to the blend without diamine cross-linker (**P2F2M** TPE), the **P2F2M** TPV displayed two DTG peaks (Fig. S14) because the rubber phases in **P2F2M** TPV were cross-linked with HMDC during the dynamic vulcanization. Therefore, the first DTG peak (T_{max1}) corresponded to thermal decomposition at a lower temperature (i.e., NR), and the second DTG peak (T_{max2}) corresponded to thermal decomposition at a higher temperature (i.e., PVDF, FKM, or FKM-MGNR). Also, it is believed that FKM is crosslinked with MGNR with diamine (as discussed earlier), resulting in improved thermal stability of the rubber phase. Interestingly, the initial decomposition temperatures ($T_{5\%}$), $T_{30\ \%}$, and $T_{50\ \%}$ of all TPVs increased with FKM and PVDF. As a result, the heat resistance indexes (T_{HRI}) were enhanced for the blends with PVDF and FKM, indicating that the incorporation of fluorinated polymer and dynamic vulcanization significantly improved the thermal stability and heat resistance of TPVs.

Furthermore, the thermostability improvement can be observed from T_{max} and T_f. It can be seen that the first (T_{max1}) and second (T_{max2}) temperatures at maximum decomposition rate, and T_f shifted to a higher temperature, and those parameters are higher than for the neat polymers. For example, T_{max1} and T_f of **P0F4M** TPV were higher than those of neat MGNR. At the same time, T_{max2}s and T_fs of **P2F2M** and **P4F0M** blends were higher than those of neat PVDF and FKM. The improved thermal properties of the TPVs result from fluorine-containing polymers and diamine cross-linking. Importantly, **5P2F2M** and **4P2F2M** showed higher T_{max2}s and T_fs than those of **5P4F0M** and **4P4F0M** TPVs, indicating a synergistic effect from the three blend components and cross-linked rubber phases.

3.7. Shape memory behavior

The shape memory behavior of this ternary blend was analyzed by U-shape bending, as shown in Figs. S15, S16, and S17. The TPV strip was bent while hot, and a temporary shape was obtained by cooling it in the ice bath. Then, the temporary shape returned almost to the original shape when heated again in the hot stage. It is observed that the original shape (strip shape) of PVDF/FKM/MGNR TPV can be well fixed to a

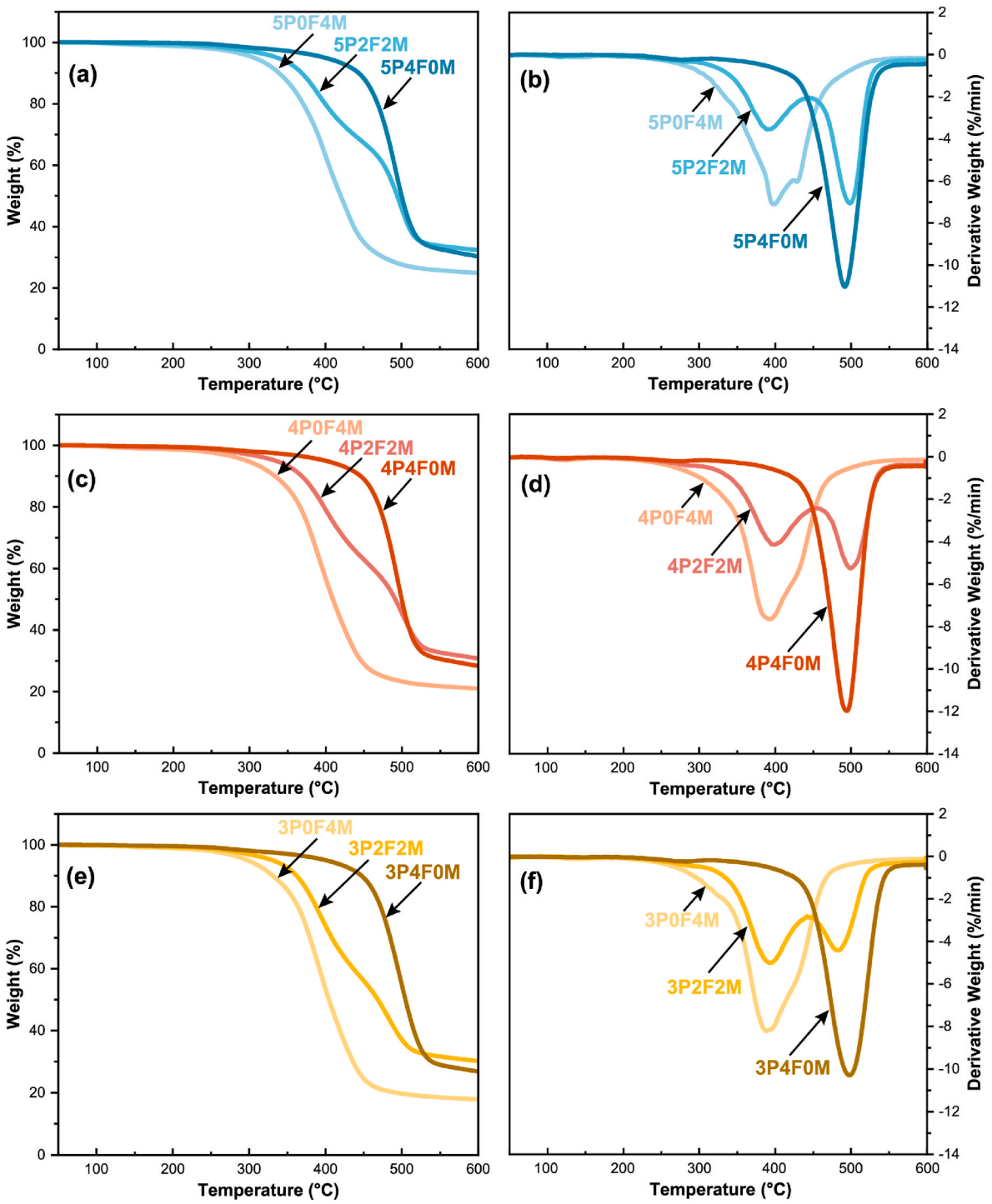

Fig. 12. TGA and DTG curves of PVDF/FKM/MGNR TPV with different blend ratios (a, b) 50%wt PVDF (**5P**), (c, d) 40%wt PVDF (**4P**), and (e, f) 30%wt PVDF (**3P**).

temporary shape (U-bent shape). After heating in the water bath, the temporary shape recovered to a permanent shape due to the elasticity provided by the rubber domains in TPV.

Shape memory characteristics of PVDF/FKM/MGNR blend are summarized in Fig. 13(a) and (b). It is clearly seen that the R_f of the blends is almost 100 %, especially for MGNR-rich blends (i.e., **P0F4M**, **P1F3M,** and **P2F2M)** because of the stiffness of PVDF and grafted PMMA domains. When the sample is cooled down, the crystallinity of PVDF and vitrification of grafted PMMA favor hardening and help maintain temporary shape, resulting in excellent shape-fixing ability. However, the R_f of **P4F0M** TPVs is slightly reduced to 90 % (Table S2). The difference in R_f between **P0F4M** and **P4F0M** TPVs is ascribed to glassy PMMA copolymer. The blend with high MGNR (**P0F4M)** results in vitrification at low temperatures. The **P0F4M** contains both crystalline segments in PVDF and glassy PMMA hard phases for shape fixation and programming process. Both regions in TPV are important for "locking". Hence, **P0F4M** TPV can be fixed very well by quenching at 5 °C. In contrast, **P4F0M** TPV displayed lower R_f than **P0F4M** TPV due to an insufficient shape fixation provided only by the PVDF hard phase. According to this, the ternary blends exhibit relatively good shape fixity and programmability.

Similarly, the recovery ratio (R_r) also was blend ratio dependent, as

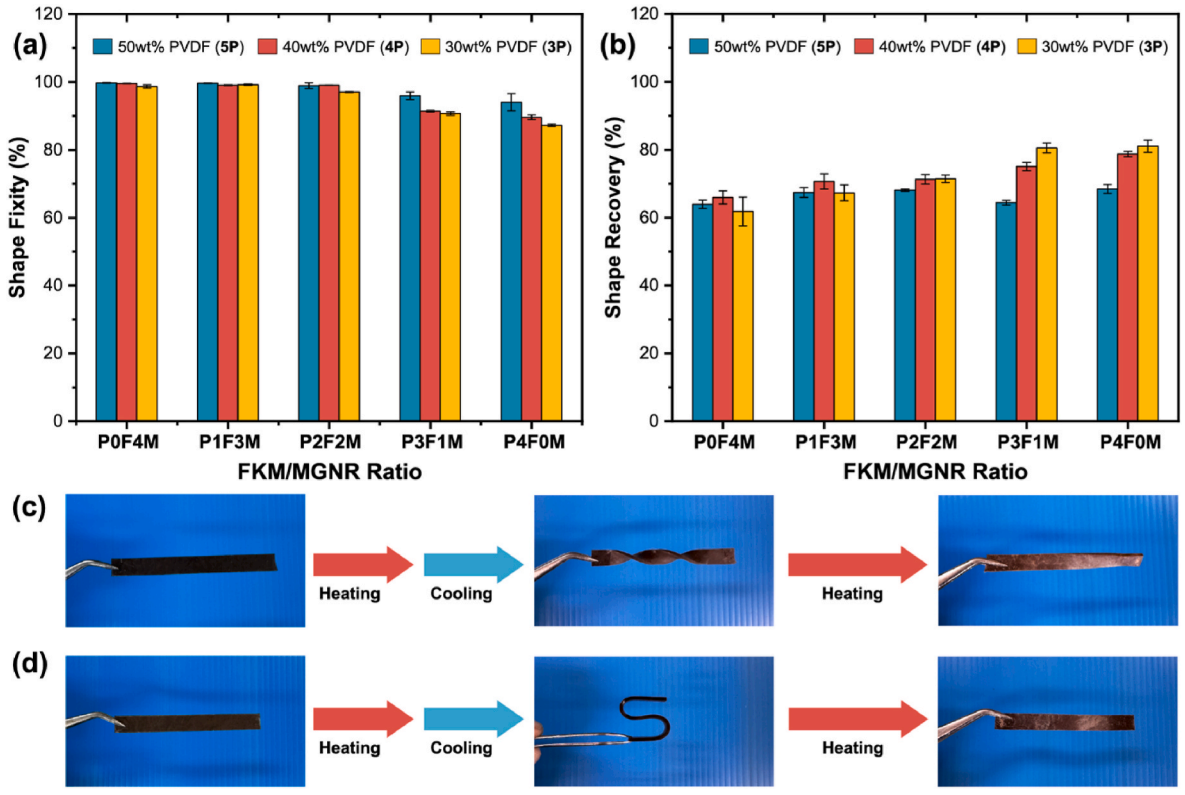

Fig. 13. (a) Fixity and (b) recovery ratio of PVDF/FKM/MGNR TPVs with different blend ratios. (c and d) Shape-memory photographs of **4P3F1M** sample.

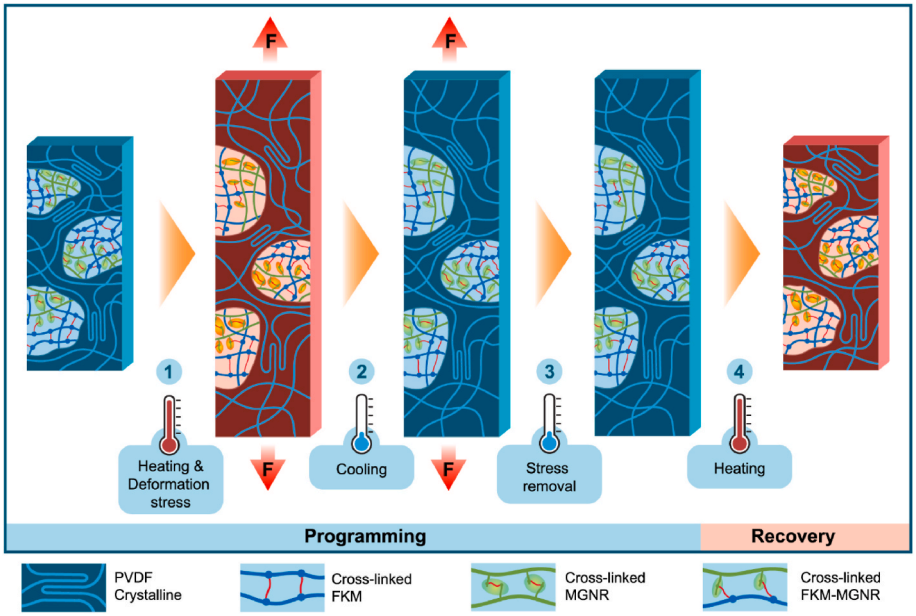

Fig. 14. An expected mechanism for the thermo-responsive SMP based on PVDF/FKM/MGNR ternary TPV.

shown in Fig. 13(b). It can be observed that R_r increased with FKM content in the blend. For example, the recovery rate of **P4F0M** TPV was 70–80 %, whereas **P0F4M** TPV offered R_r of only ~60 %. As mentioned earlier, grafted PMMA domains can act as switch domains and prevent shape recovery due to their vitrification in the glassy state. Therefore, the recovery of **P0F4M** was impeded by grafted PMMA domains. The R_r was significantly improved by the FKM domain because the cross-linked network in FKM provides the driving force for recovery [7,23,67]. Fan et al. also found that the shape recovery of TPV-containing FKM was significantly better than that of TPV without FKM, and the shape recovery ratio at 100 °C was also in the range of 60–80 % [36]. As expected, the R_r for ternary blends (i.e., **1F3M**, **2F2M**, and **3F1M**) was between those of PVDF/MGNR and PVDF/FKM TPVs. Although these ternary blends demonstrated shape recovery lower than 90 %, their excellent programmability and temporary shape can be maintained for a long time. At the same time, the optimized shape memory performance from these ternary TPVs was at a similar level as that of other binary TPVs [47,68] and other PVDF blends [48,69,70].

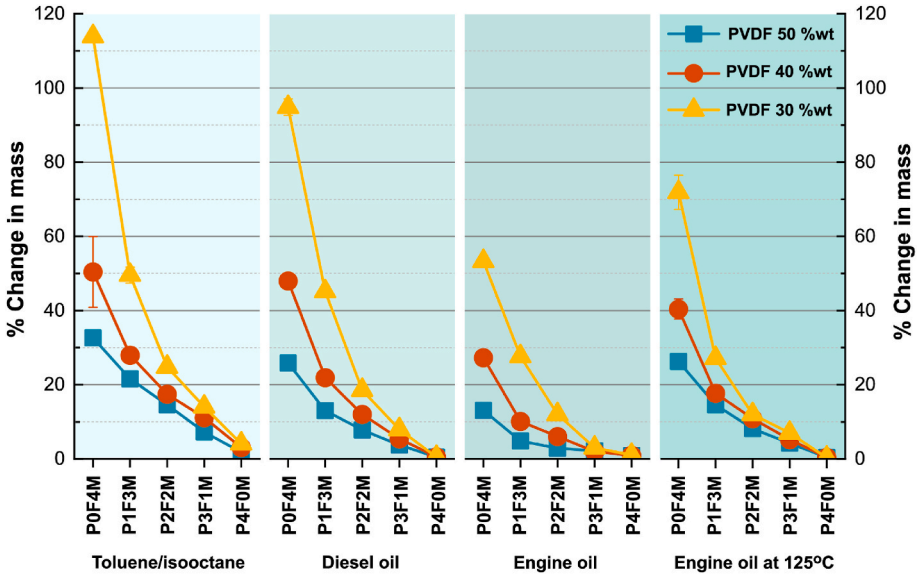

Fig. 15. Weight change of the ternary PVDF/FKM/MGNR blend in different liquids.

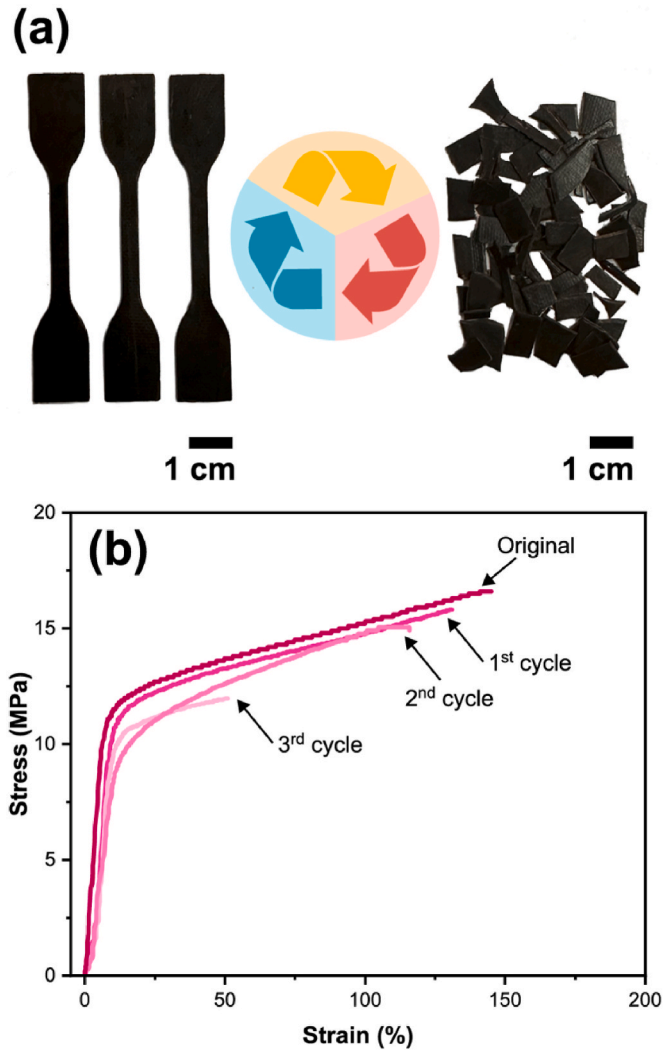

Fig. 16. Recyclability of ternary TPV based on PVDF/FKM/MGNR blend (**4F2F2M**).

As an amusement, the strips of ternary **4P3F1M** TPV were deformed into various shapes (i.e., bending or twisting) to demonstrate the shape memory performance (Fig. 13(c) and (d)). The TPV strips certainly remained in the programmed shape, and they can extensively recover the original shape quickly from diverse deformations. Hence, these features are sufficient to make them cases of smart elastomeric materials. A schematic illustration of the programming and recovery ability of the PVDF/FKM/MGNR ternary TPV is presented in Fig. 14. Generally, the shape memory behavior of a thermoplastic elastomer is mainly contributed by soft (i.e., rubber-like networks and chemical crosslinks) and hard (i.e., crystalline and glassy states) domains. In this system, the crystalline domains of PVDF, glassy regions of MGNR, and crosslinked FKM-MGNR are fully responsible for the shape memory effect. In the beginning, crystalline PVDF was partly melted, and grafted PMMA softened when reaching ~100 °C (T_{trans}). The sample can be deformed and stretched to fix the shape. Freezing the deformed shape below T_{trans}, the solidification temperature of crystalline PVDF, and vitrification of grafted PMMA allow stored elastic force for fixation of deformed samples. By further reheating to T_{trans}, the thermolabile crystalline and glassy segments in the system induce recovery of the permanent shape, owing to stress release in soft rubber networks as well as cross-linked FKM, cross-linked MGNR, and cross-linked FKM-MGNR networks.

3.8. Swelling resistance and recyclability

PVDF and FKM exhibit excellent oil resistance because of their polar chemical structure and fluorine atoms in the backbone. Therefore, the effects of the ternary blend on solvent and oil resistances were investigated. The weight changes and volume swelling of the samples after immersion in different solvents and oils are summarized in Figs. 15 and S15 respectively. Also, the oil resistance of TPV depends not only on the blend components but also on the type of solvent and temperature. Large weight changes were observed for low-viscosity solvents (i.e., toluene and isooctane) because of their low molecular weight. However, engine oil exhibits higher viscosity than toluene and isooctane. Thus, the weight changes of the TPV immersed in engine oil were lower than those with toluene and isooctane. With increasing temperature, the weight changes in engine oil increased due to molecular mobility. Regarding the influence of blend ratio, blending only PVDF with MGNR40 (i.e., **P0F4M**) showed poor oil resistance due to the non-polar and hydrocarbon structure of NR, which preferably absorbs hydrocarbon solvents and oils. In contrast, it is clear that a high PVDF content (i.e., 50 wt% PVDF

or **5P**) in TPV resulted in a lower % change in mass and volume swelling because PVDF is a semi-crystalline fluorinated thermoplastic. Hence, the crystalline structure and fluorine atoms can prevent the penetration of hydrocarbon molecules. At the same time, the incorporation of FKM into the ternary blend (i.e., **P1F3M**, **P2F2M**, and **P3F1M**) or binary blend (**P4F0M**) caused reduced swelling of the samples (low weight change and volume swelling). The ternary TPV based on PVDF/FKM/MGNR blend (**P2F2M**) in this work demonstrated low mass change (<20 %) and volume swelling (<40 %), which are comparable in oil resistance to other TPVs reported in the literature [40,71,72]. The solvent and oil resistance results indicate that the combination of PVDF and FKM in ternary blend TPV provides excellent solvent and oil resistance, appropriate for automobile fuel hose application [73].

The advantageous properties of TPV are recyclability and reprocessing, which cannot be obtained from conventional rubber vulcanizates. Therefore, TPV materials and scraps can be reprocessed by thermoplastic machinery such as extruder, thermoforming, blow molding, and injection molding machines. In this study, TPV scraps were cut into small pieces and pressed by compression molding at 200 °C. As shown in Fig. 16(a), this ternary TPV (**4F2F2M**) can be recycled as thermoplastic material and is in this respect eco-friendly and sustainable. Typically, the recyclability originates from thermoplastic component in TPV. The stress-strain curves of recycled ternary and binary TPV are depicted in Figs. 16b and S16, respectively. It is clear that the recycled PVDF/FKM TPV (**4F4F0M**) exhibited better recyclability with negligible change in mechanical properties after recycling. This was mainly attributed to the heat and aging resistance of PVDF and FKM components in TPV. The mechanical properties of ternary TPVs (**4F2F2M**) were slightly reduced after recycling (Fig. 16(b)). Meanwhile, TPV based on PVDF/MGNR (**40F4M)** exhibited poor reprocessing response because tensile strength and elongation at break of recycled **40F4M** TPV were significantly deteriorated. This can be explained by the thermal degradation of NR segments in MGNR at reprocessing temperature.

4. Conclusion

In summary, high-performance TPVs with excellent mechanical properties, phase morphology, and heat and oil resistances, have been developed from ternary blends of modified NR with PVDF and FKM. The study demonstrated that the phases in the blend had significant effects on its overall performance. The PVDF/FKM/MGNR blends containing 50/50 wt% of FKM and MGNR (**P2F2M**) showed a significant improvement in tensile strength and elongation at break, which confirms good compatibility in the blend. The PVDF/FKM/MGNR presented smaller dispersed domain size than the binary PVDF/FKM and PVDF/MGNR blends. The addition of a third component in the blends facilitates achieving a finer domain size and more homogenous blends. As a result, improved mechanical properties of the ternary blend were mainly attributed to the small domains and strong interfacial adhesion. The dynamic mechanical properties also demonstrated that the incorporation of three polymers enhanced the storage modulus, whereas the loss tangent (tan δ) peak of each component obviously shifted toward each other, indicating the synergistic effects in the ternary blend and good compatibility. Moreover, the dipole-dipole interactions provided by the introduction of MGNR into the ternary blend caused reduced crystallization and melting temperatures of PVDF due to imperfect crystallization. The PVDF/FKM/MGNR TPV can also exhibit shape memory behavior with good shape fixity and recovery because grafted PMMA in MGNR acts as a switch domain, and FKM and NR backbones act as net points. In addition, heat and oil resistances of the PVDF/FKM/MGNR TPV improved with FKM and PVDF contents due to the polar fluorine atoms in the main chains. Notably, our studies revealed that the extraordinary performance with smart properties, heat, and solvent resistance of ternary PVDF/FKM/MGNR TPV can be appropriate for applications in the automotive sector and advanced elastomeric materials.

CRediT authorship contribution statement

Subhan Salaeh: Writing – review & editing, Writing – original draft, Project administration, Investigation, Funding acquisition, Conceptualization. **Anoma Thitithammawong:** Writing – review & editing. **Shib Shankar Banerjee:** Writing – review & editing, Writing – original draft.

Declaration of competing interest

The authors declare that we have no known competing financial interests or personal relationships that could have appeared to influence the work reported in this paper.

Data availability

The data that has been used is confidential.

Acknowledgements

This research was supported by the National Science, Research and Innovation Fund (NSRF) and Prince of Songkla University (SAT6505064S). S.S. thanks Ms. Puntira Kao-ian for sample preparation and CS Rubber Industry Co., Ltd. for FKM rubber.

Appendix B. Supplementary data

Supplementary data to this article can be found online at https://doi.org/10.1016/j.polymertesting.2024.108594.

References

[1] K.-J. Li, C. Wang, T.-T. Zheng, F. Zhao, M.-C. Luo, S. Liao, Towards high performance anti-aging diolefin elastomers based on structure healing strategy, Polymer 186 (2020) 122076.
[2] X. Chen, H.-F. Zhang, K.-J. Li, S. Liao, M.-C. Luo, Enabling superior thermo–oxidative resistance elastomers based on a structure recovery strategy, Macromol. Rapid Commun. 42 (2021) 2000762.
[3] C.K.L. Davies, S.V. Wolfe, I.R. Gelling, A.G. Thomas, Strain crystallization in random copolymers produced by epoxidation of cis 1,4-polyisoprene, Polymer 24 (1983) 107–113.
[4] C.S.L. Baker, I.R. Gelling, R. Newell, Epoxidized natural rubber, Rubber Chem. Technol. 58 (1985) 67–85.
[5] B.V. Quevedo, D. Komatsu, M. de Lourdes Rezende, E.A. de Rezende Duek, Synthesis of epoxidized natural rubber grafted with hyaluronic acid for the development of biomaterials, Int. J. Biol. Macromol. 244 (2023) 125359.
[6] D. Derouet, Q.N. Tran, J.L. Leblanc, Physical and mechanical properties of poly (methyl methacrylate)-grafted natural rubber synthesized by methyl methacrylate photopolymerization initiated by N,N-diethyldithiocarbamate functions previously created on natural rubber chains, J. Appl. Polym. Sci. 112 (2009) 788–799.
[7] S. Salaeh, S. Nobnop, B. Thongnuanchan, A. Das, S. Wießner, Thermo-responsive programmable shape memory polymer based on amidation cured natural rubber grafted with poly(methyl methacrylate), Polymer 262 (2022) 125444.
[8] S. Kawahara, H. Nishioka, M. Yamano, Y. Yamamoto, Synthetic rubber with the tensile strength of natural rubber, ACS Appl. Polym. Mater. 4 (2022) 2323–2328.
[9] P. Piya-areetham, P. Prasassarakich, G.L. Rempel, Organic solvent-free hydrogenation of natural rubber latex and synthetic polyisoprene emulsion catalyzed by water-soluble rhodium complexes, J. Mol. Catal. A Chem. 372 (2013) 151–159.
[10] P. Piya-areetham, G.L. Rempel, P. Prasassarakich, Hydrogenated nanosized polyisoprene as a thermal and ozone stabilizer for natural rubber blends, Polym. Degrad. Stabil. 102 (2014) 112–121.
[11] N. Wu, H. Zhang, G. Fu, Super-tough poly(lactide) thermoplastic vulcanizates based on modified natural rubber, ACS Sustain. Chem. Eng. 5 (2017) 78–84.
[12] S. Salaeh, T. Banda, V. Pongdong, S. Wießner, A. Das, A. Thitithammawong, Compatibilization of poly(vinylidene fluoride)/natural rubber blend by poly (methyl methacrylate) modified natural rubber, Eur. Polym. J. 107 (2018) 132–142.
[13] S.S. Banerjee, A.K. Bhowmick, High-temperature thermoplastic elastomers from rubber–plastic blends: a state-of-the-art review, Rubber Chem. Technol. 0 (2017) null.
[14] N. Ning, S. Li, H. Wu, H. Tian, P. Yao, G.-H. Hu, M. Tian, L. Zhang, Preparation, microstructure, and microstructure-properties relationship of thermoplastic vulcanizates (TPVs): a review, Prog. Polym. Sci. 79 (2018) 61–97.

[15] M. Mondal, U. Gohs, U. Wagenknecht, G. Heinrich, Additive free thermoplastic vulcanizates based on natural rubber, Mater. Chem. Phys. 143 (2013) 360–366.
[16] S. Rooj, V. Thakur, U. Gohs, U. Wagenknecht, A.K. Bhowmick, G. Heinrich, In situ reactive compatibilization of polypropylene/epoxidized natural rubber blends by electron induced reactive processing: novel in-line mixing technology, Polym. Adv. Technol. 22 (2011) 2257–2263.
[17] P. Sae-Oui, C. Sirisinha, P. Sa-nguanthammarong, P. Thaptong, Properties and recyclability of thermoplastic elastomer prepared from natural rubber powder (NRP) and high density polyethylene (HDPE), Polym. Test. 29 (2010) 346–351.
[18] M. Rezaei Abadchi, A. Jalali Arani, H. Nazockdast, Partial replacement of NR by GTR in thermoplastic elastomer based on LLDPE/NR through using reactive blending: its effects on morphology, rheological, and mechanical properties, J. Appl. Polym. Sci. 115 (2010) 2416–2422.
[19] R. Asaletha, M.G. Kumaran, S. Thomas, Thermoplastic elastomers from blends of polystyrene and natural rubber: morphology and mechanical properties, Eur. Polym. J. 35 (1999) 253–271.
[20] D. Yuan, Z. Chen, C. Xu, K. Chen, Y. Chen, Fully biobased shape memory material based on novel cocontinuous structure in poly(lactic acid)/natural rubber TPVs fabricated via peroxide-induced dynamic vulcanization and in situ interfacial compatibilization, ACS Sustain. Chem. Eng. 3 (2015) 2856–2865.
[21] D. Yuan, J. Ding, W. Mou, Y. Wang, Y. Chen, Bio-based polylactide/epoxidized natural rubber thermoplastic vulcanizates with a co-continuous phase structure, Polym. Test. 64 (2017) 200–206.
[22] L.-F. Ma, R.-Y. Bao, R. Dou, Z.-Y. Liu, W. Yang, B.-H. Xie, M.-B. Yang, Q. Fu, A high-performance temperature sensitive TPV/CB elastomeric composite with balanced electrical and mechanical properties via PF-induced dynamic vulcanization, J. Mater. Chem. A 2 (2014) 16989–16996.
[23] S. Salaeh, A. Das, S. Wießner, Design and fabrication of thermoplastic elastomer with ionic network: a strategy for good performance and shape memory capability, Polymer 223 (2021) 123699.
[24] X. Hu, H. Kang, Y. Li, Y. Geng, R. Wang, L. Zhang, Preparation, morphology and superior performances of biobased thermoplastic elastomer by in situ dynamical vulcanization for 3D-printed materials, Polymer 108 (2017) 11–20.
[25] Z. Cui, L. Wei, Y. Liu, A. Du, Systematic investigation on the effect of processing procedures on the performance of oil-resistant thermoplastic vulcanizates based on HNBR/TPEE, J. Appl. Polym. Sci. 140 (2023) e53860.
[26] H.S. Jung, M.C. Choi, Y.-W. Chang, P.-H. Kang, S.C. Hong, Facile preparation of thermoplastic elastomer with high service temperature from dry selective curing of compatibilized EPDM/polyamide-12 blends, Eur. Polym. J. 66 (2015) 367–375.
[27] A. Datta Sarma, H.R. Padmanathan, S. Saha, S. Shankar Banerjee, A.K. Bhowmick, Design and properties of a series of high-temperature thermoplastic elastomeric blends from polyamides and functionalized rubbers, J. Appl. Polym. Sci. 134 (2017) 45353.
[28] G. Tillet, G. Lopez, M.-H. Hung, B. Améduri, Crosslinking of fluoroelastomers by “click” azide–nitrile cycloaddition, J. Polym. Sci. A Polym. Chem. 53 (2015) 1171–1173.
[29] Y. Guo, H. Tian, X. Li, J. Han, N. Ning, M. Tian, L. Zhang, Preparation of FKM/EFEP thermoplastic vulcanizate with excellent heat and oil resistance, gas barrier property and recyclability, Polymer 262 (2022) 125429.
[30] S. Saha, A.K. Bhowmick, Computer aided simulation of thermoplastic elastomer from poly (vinylidene fluoride)/hydrogenated nitrile rubber blend and its experimental verification, Polymer 112 (2017) 402–413.
[31] Y. Wang, X. Jiang, C. Xu, Z. Chen, Y. Chen, Effects of partial replacement of silicone rubber with flurorubber on properties of dynamically cured poly(vinylidene fluoride)/silicone rubber/flurorubber ternary blends, Polym. Test. 32 (2013) 1392–1399.
[32] P. Kao-ian, S.S. Banerjee, S. Yudha S, S. Salaeh, Strengthened poly(vinylidene fluoride)/epoxidized natural rubber blend by a reactive compatibilizer based on an amino acid-modified fluorocarbon elastomer, Ind. Eng. Chem. Res. 63 (2024) 6615–6631.
[33] S. Salaeh, Processing of natural rubber composites and blends: relation between structure and properties, in: Université Claude Bernard Lyon 1, Prince of Songkla University, 2014.
[34] S. Salaeh, P. Cassagnau, G. Boiteux, S. Wießner, C. Nakason, Thermoplastic vulcanizates based on poly(vinylidene fluoride)/Epoxidized natural rubber blends: effects of phenolic resin dosage and blend ratio, Mater. Chem. Phys. 219 (2018) 222–232.
[35] S. Salaeh, G. Boiteux, P. Cassagnau, C. Nakason, Dynamically cured poly (vinylidene fluoride)/epoxidized natural rubber blends filled with ferroelectric ceramic barium titanate, Compos. Part A-Appl. S. 93 (2017) 107–116.
[36] J. Fan, M. Yan, J. Huang, L. Cao, Y. Chen, Fabrication of smart shape memory fluorosilicon thermoplastic vulcanizates: the effect of interfacial compatibility and tiny crystals, Ind. Eng. Chem. Res. 58 (2019) 15199–15208.
[37] S.S. Banerjee, A.K. Bhowmick, Novel nanostructured polyamide 6/fluoroelastomer thermoplastic elastomeric blends: influence of interaction and morphology on physical properties, Polymer 54 (2013) 6561–6571.
[38] J. Nunes-Pereira, P. Sharma, L.C. Fernandes, J. Oliveira, J.A. Moreira, R.K. Sharma, S. Lanceros-Mendez, Poly(vinylidene fluoride) composites with carbon nanotubes decorated with metal nanoparticles, Compos. Part B-Eng. 142 (2018) 1–8.
[39] K. Asai, M. Okamoto, K. Tashiro, Crystallization behavior of nano-composite based on poly(vinylidene fluoride) and organically modified layered titanate, Polymer 49 (2008) 4298–4306.
[40] S. Khanra, A. Kumar, D. Ganguly, S.K. Ghorai, S. Chattopadhyay, The efficacy of methyl vinyl silicone-g-maleic anhydride in the compatibilization of fluoroelastomer and silicone based super specialty elastomer blend, J. Polym. Res. 29 (2022) 174.
[41] S.S. Banerjee, U. Gohs, C. Zschech, G. Heinrich, Design and properties of high-performance polyamide 6/fluoroelastomer blends by electron-induced reactive processing, Eur. Polym. J. 85 (2016) 508–518.
[42] X. Cui, J. Chen, Y. Zhu, W. Jiang, Natural sunlight-actuated shape memory materials with reversible shape change and self-healing abilities based on carbon nanotubes filled conductive polymer composites, Chem. Eng. J. 382 (2020) 122823.
[43] S.S. Banerjee, K.D. Kumar, A.K. Sikder, A.K. Bhowmick, Nanomechanics and origin of rubber elasticity of novel nanostructured thermoplastic elastomeric blends using atomic force microscopy, Macromol. Chem. Phys. 216 (2015) 1666–1674.
[44] S. Mitra, A. Ghanbari-Siahkali, P. Kingshott, K. Almdal, H. Kem Rehmeier, A. G. Christensen, Chemical degradation of fluoroelastomer in an alkaline environment, Polym. Degrad. Stabil. 83 (2004) 195–206.
[45] P. Awasthi, S.S. Banerjee, Design of ultrastretchable and super-elastic tailorable hydrophilic thermoplastic elastomeric materials, Polymer 252 (2022) 124914.
[46] B. Lu, K. Lamnawar, A. Maazouz, H. Zhang, Revealing the dynamic heterogeneity of PMMA/PVDF blends: from microscopic dynamics to macroscopic properties, Soft Matter 12 (2016) 3252–3264.
[47] J. You, H. Fu, W. Dong, L. Zhao, X. Cao, Y. Li, Shape memory performance of thermoplastic polyvinylidene fluoride/acrylic copolymer blends physically cross-linked by tiny crystals, ACS Appl. Mater. Interfaces 4 (2012) 4825–4831.
[48] J. You, W. Dong, L. Zhao, X. Cao, J. Qiu, W. Sheng, Y. Li, Crystal orientation behavior and shape-memory performance of poly(vinylidene fluoride)/acrylic copolymer blends, J. Phys. Chem. B 116 (2012) 1256–1264.
[49] A. Taguet, B. Ameduri, B. Boutevin, Grafting of commercially available amines bearing aromatic rings onto poly(vinylidene-co-hexafluoropropene) copolymers, J. Polym. Sci. A Polym. Chem. 44 (2006) 1855–1868.
[50] C.F. Antunes, M. van Duin, A.V. Machado, Morphology and phase inversion of EPDM/PP blends - effect of viscosity and elasticity, Polym. Test. 30 (2011) 907–915.
[51] P. Xu, P. Ma, X. Cai, S. Song, Y. Zhang, W. Dong, M. Chen, Selectively cross-linked poly (lactide)/ethylene-glycidyl methacrylate-vinyl acetate thermoplastic elastomers with partial dual-continuous network-like structures and shape memory performances, Eur. Polym. J. 84 (2016) 1–12.
[52] T.S. Omonov, C. Harrats, G. Groeninckx, P. Moldenaers, Anisotropy and instability of the co-continuous phase morphology in uncompatibilized and reactively compatibilized polypropylene/polystyrene blends, Polymer 48 (2007) 5289–5302.
[53] Y.K. Chen, Z. Gong, L.M. Cao, Y.H. Wang, D.S. Yuan, C.H. Xu, Novel fluorosilicone thermoplastic vulcanizates prepared via core-shell dynamic vulcanization: effect of fluororubber/silicone rubber ratio on morphology, crystallization behavior, and mechanical properties, Polym. Adv. Technol. 29 (2018) 1456–1468.
[54] H. Wang, Z. Fu, W. Dong, Y. Li, J. Li, Formation of interfacial janus nanomicelles by reactive blending and their compatibilization effects on immiscible polymer blends, J. Phys. Chem. B 120 (2016) 9240–9252.
[55] V. Thakur, U. Gohs, U. Wagenknecht, G. Heinrich, Electron-induced reactive processing of thermoplastic vulcanizate based on polypropylene and ethylene propylene diene terpolymer rubber, Polym. J. 44 (2012) 439–448.
[56] J.N. Martins, T.S. Bassani, R.V.B. Oliveira, Morphological, viscoelastic and thermal properties of poly(vinylidene Fluoride)/POSS nanocomposites, Mater. Sci. Eng. C 32 (2012) 146–151.
[57] V. Sencadas, S. Lanceros-Mendez, R.S.I. Serra, A.A. Balado, J.L.G. Ribelles, Relaxation dynamics of poly(vinylidene fluoride) studied by dynamical mechanical measurements and dielectric spectroscopy, Eur. Phys. J. E 35 (2012).
[58] Y. Li, Y. Iwakura, H. Shimizu, Polymer crystallites with few tie molecules from a miscible polymer blend, Macromolecules 41 (2008) 3396–3400.
[59] Y. Li, Y. Iwakura, L. Zhao, H. Shimizu, Nanostructured poly(vinylidene fluoride) materials by melt blending with several percent of acrylic rubber, Macromolecules 41 (2008) 3120–3124.
[60] F.A. Landis, S.R. March, D. Deivasagayam, R.T. Mathers, Crystallization of Poly (vinylidene fluoride) in Blends with Poly(methyl methacrylate-co-methacrylic acid) Copolymers, Macromol. Chem. Phys. 215 (2014) 153–162.
[61] D.-J. Lin, C.-L. Chang, C.-K. Lee, L.-P. Cheng, Preparation and characterization of microporous PVDF/PMMA composite membranes by phase inversion in water/DMSO solutions, Eur. Polym. J. 42 (2006) 2407–2418.
[62] E. Afonso, A. Martínez-Gómez, P. Tiemblo, N. García, Exploring chemical and structural features to tailor wetting properties of PVDF and PVDF/PMMA surfaces, Polymer 262 (2022) 125441.
[63] A. De Neef, C. Samuel, H. Amorín, G. Stoclet, R. Jiménez, P. Dubois, J. Soulestin, J.-M. Raquez, Beta phase crystallization and ferro- and piezoelectric performances of melt-processed poly(vinylidene difluoride) blends with poly(methyl methacrylate) copolymers containing ionizable moieties, ACS Appl. Polym. Mater. 2 (2020) 3766–3780.
[64] K. Zhang, V. Nagarajan, M. Misra, A.K. Mohanty, Supertoughened renewable PLA reactive multiphase blends system: phase morphology and performance, ACS Appl. Mater. Interfaces 6 (2014) 12436–12448.
[65] Y. Wang, L. Fang, C. Xu, Z. Chen, Y. Chen, Morphology and properties of poly (vinylidene fluoride)/silicone rubber blends, J. Appl. Polym. Sci. 131 (2014).
[66] E. Savonnet, E. Grau, S. Grelier, B. Defoort, H. Cramail, Divanillin-based epoxy precursors as DGEBA substitutes for biobased epoxy thermosets, ACS Sustain. Chem. Eng. 6 (2018) 11008–11017.
[67] Y. Zheng, J. Qin, J. Shen, S. Guo, Controllable distribution of conductive particles in polymer blends via a bilayer structure design: a strategy to fabricate shape-memory composites with tunable electro-responsive properties, J. Mater. Chem. C 8 (2020) 9593–9601.

[68] J. Fan, J. Huang, L. Cao, S. Yin, Y. Chen, Mechanically robust, reprocessable shape memory fluorosilicon materials using β-H elimination reaction and in situ interfacial compatibilization, Ind. Eng. Chem. Res. 59 (2020) 12745–12754.
[69] Z. Shi, G. Zhao, G. Wang, L. Zhang, C. Wei, J. Chai, Development of ultralight, tough and hydrophobic polymethylmethacrylate/polyvinylidene fluoride shape memory foams for heat insulation applications, Mater. Des. 225 (2023) 111527.
[70] X. Ji, D. Chen, Y. Zheng, J. Shen, S. Guo, E. Harkin-Jones, Multilayered assembly of poly(vinylidene fluoride) and poly(methyl methacrylate) for achieving multi-shape memory effects, Chem. Eng. J. 362 (2019) 190–198.
[71] W. Wu, C. Wan, S. Wang, Y. Zhang, Reactive processing of ethylene-vinyl acetate rubber/polyamide blends via a dynamic transesterification reaction, Polym. Bull. 71 (2014) 1505–1521.
[72] Z. Cui, J. Wang, L. Wei, Y. Liu, A. Du, Effect of dynamic vulcanization time on the performance of thermoplastic vulcanizates based on hydrogenated acrylonitrile butadiene rubber/thermoplastic polyester elastomer, J. Appl. Polym. Sci. 140 (2023) e54703.
[73] W. Wu, B. Jin, H. Xu, H. Wu, Z. Yuan, Z. Xie, Y. Wen, K. Wang, J. Wu, Low-fuel-permeation thermoplastic vulcanizates prepared from mutually miscible fluoroelastomer and poly(vinylidene fluoride–hexafluoropropylene), Polym. Int. 72 (2023) 822–831.